Wave mediated interaction in a lattice of bouncing drops

A Thesis

submitted to

Indian Institute of Science Education and Research Pune
in partial fulfillment of the requirements for the

BS-MS Dual Degree Programme
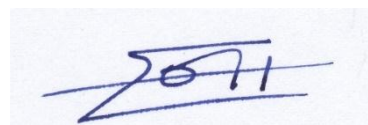
by

Surabhi K S

IISER PUNE

Indian Institute of Science
Education and Research Pune

Dr. Homi Bhabha Road, Pashan, Pune 411008, INDIA.

April, 2019

Certificate

This is to certify that this dissertation entitled **Wave mediated interaction in a lattice of bouncing drops**, towards the partial fulfilment of the BS-MS dual degree programme at the Indian Institute of Science Education and Research, Pune represents study/work carried out by **SURABHI K S** at the Langevin Institute under the supervision of **Dr. Emmanuel Fort,** École supérieure de physique et de chimie industrielles de la Ville de Paris (ESPCI), Paris during the academic year 2018-2019.

Dr. Emmanuel Fort

Committee:

Dr. Emmanuel Fort

Dr. Bhas Bapat

I dedicate this thesis to IISER Pune,

for being my home for all these years and an integral part of me.

Declaration

I hereby declare that the matter embodied in the report entitled **Wave mediated interaction in a lattice of bouncing drops** are the results of the work carried out by me at Langevin Institute, Paris, under the supervision of **Dr. Emmanuel Fort** and the same has not been submitted elsewhere for any other degree.

Surabhi K S

Acknowledgements

I would like to thank PMMH, ESPCI and CNRS for funding my project. I would also like to thank my host laboratory, Institut Langevin wherein I carried out all the experiments.

I would like to thank Prof. Emmanuel Fort for giving me an opportunity to work on this project and the amazing discussions that ensued. I would also like to thank Dr. Antonin Eddi for giving me an opportunity with the first part of the internship and for his insights into the project and key aspects of analysis. I am extremely grateful for all the help and guidance from Sander, and for all the discussions. I thank Guillaume for his help and company!

I would like to thank Prof. Bhas Bapat for his constant support throughout my stay at IISER and during the course of my project, and his key insights into the project. None of this would have been possible without him.

This project would not have been possible without the support of Prof. G. Ambika, Prof. Mukul Kabir, Prof. Umakant Rapol and Prof. Anirban Hazra.

I would like to thank Sneha Chordiya Madam and Priyadarshini Tamhane Madam from the administration section, who helped me with so many documents throughout the year. Their timely help was instrumental to my project performance.

I would like to thank Campus France and Charpak for giving me the first opportunity to work at Institut Langevin, and the CNRS lab in India for their support last year. I would like to thank the applied mathematics department at Cambridge for giving me an opportunity and bursary to attend the Third Edwards symposium along with recognizing the work and awarding the poster prize.

Most of all I would like to thank IISER, my home for the past five years and my friends. I would like to thank Deepak Sharma for being my contact from IISER, during the course of last year.

And finally I would like to thank my family who have always been there for me and supported me in every way possible.

Abstract

This project's larger goal involves devising an experimental method to investigate links between a lattice of bouncing drops and the Ising machine. The coupling between droplets plays a crucial role in this aspect and the work carried out here encapsulates some major features pertaining to this interaction between droplets.

An Ising machine is an artificial system of spins based on the Ising model, which describes the energy of a set of interacting constituent spin like elements with bi-stable states. Combinatorial optimization problems are a large class of problems which involve optimizing a certain quantity from a set of discrete elements and they can be mapped to the Hamiltonian function of the Ising model. These problems belong to the class of NP-hard problems for which computational complexity grows as a power law with each new added element. The purpose of building an Ising machine is to provide an architecture which can efficiently solve such problems by finding the ground state of its constituent elements. Previously, interacting coupled parametric oscillators have been proposed as a possible implementation of an Ising machine. The ground state can be efficiently determined by slowly increasing the excitation until each oscillator reaches a bi-stable state which is determined by its interactions with the other oscillators.

A set of bouncing droplets on a vertically vibrated bath is a good candidate for an Ising machine. Each droplet can be considered as a parametrical oscillator which is controlled by the vibration of the bath. These droplets undergo period doubling above a given excitation threshold which defines a bi-stable state defined by their phase. These 'artificial spins' interact with each other through the waves that they emit on the bath. This interaction can be tuned by changing the distances between droplets.

This project aims to experimentally analyse the analogy between Ising machine and bouncing droplets by looking at their dynamics and interaction. We develop a novel technique to produce reproducible drops (0.64 mm in diameter). We fully characterize the period doubling transition for one droplet and its associated wave field emission. This gives new insight for further analysis involving looking at the Fourier components of the wave field and understanding how droplets reach the ground state. We study the interaction and relative phase selection for a two droplets systems and showed that it finds the minimum energy state of the conformational space depending on their mutual interaction. Finally, we show some examples of more complex sets of interacting

droplets which also attain ground states. These results show that interacting droplets contain many features of an Ising machine and can perform relevant optimization calculations. The full experimental characterizations can now be used to perform realistic simulations and to develop an Ising model based on this system.

Table of Contents

1 Introduction

In this report we use a lattice of bouncing dropletsm bouncing on a vibrated bath and look at the interaction through the waves they produce. This system can be viewed as a set of interacting parametrically excited oscillators. For sufficient excitation, the bouncing droplets undergo period doubling wherein they alternate between a long and short bounce. This defines two possible states depending on their relative phase for each droplet. In our regime of operation, the system resembles a set of interacting spins which are usually described by the Ising model. There is a strong interest in artificially engineered systems that can be described by the Ising model. These systems are called Ising machines. They can be used as smart computing architectures to solve complex optimization problems. Since optimization problems can be mapped onto the Ising model. Hence, finding the ground state of an Ising machine is equivalent to solving the optimization problem.

The bouncing droplet system is very complex and involves hydrodynamic processes that have not been fully understood in the context of their transition to a bi-stable state. A model for the wave generation, droplet dynamics and their coupling is still needed to fully understand the dynamics of the system and gauge as to what extent it could solve problems and be considered as an Ising machine. This work is a comprehensive experimental study of the droplet system. It provides a full characterization of the bouncing dynamics, of the waves emitted and of the coupling between these 'artificial spins'. In addition, it gives evidence regarding the ability of this system to find the ground state.

1.1 Bouncing dynamics of a single droplet

It is found that when a bath of silicone oil is vibrated at very high frequencies like 50 Hz to 80Hz [1] to sustain droplets bouncing on the surface by the formation of an air layer, it gives rise to various interesting phenomena like [2] droplets moving on the surface called walkers, [3] particle-wave interactions, [4] single particle diffraction statistics and so on. All these experiments involve dynamics of the drop with the surface. Both the bath and the droplets are made of silicone oil.
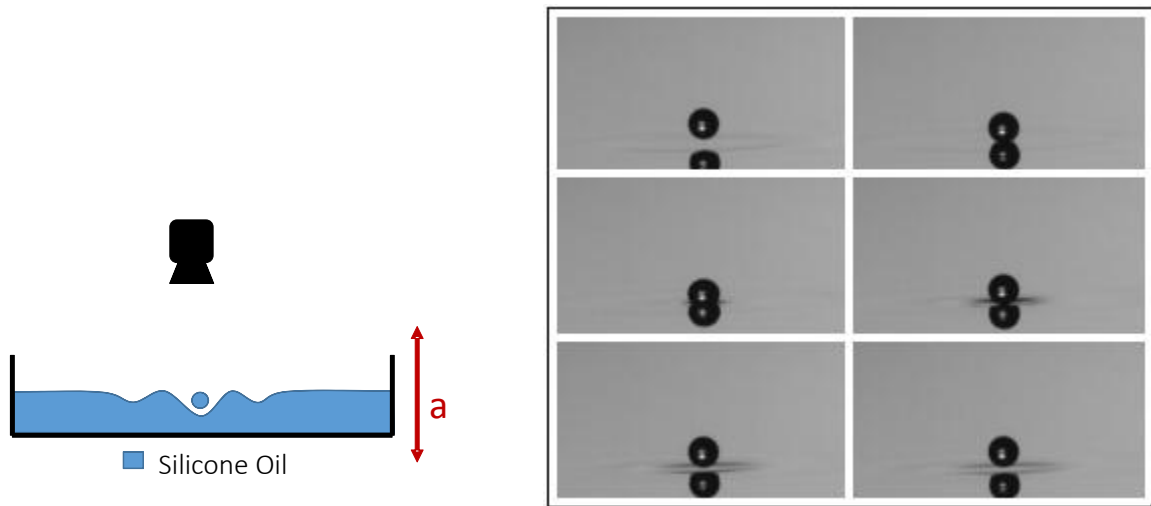

Figure 1: (Left) Silicone oil bath when excited sinusoidally with an amplitude a = Asin(ωt) gives rise to interesting phenomena. Droplets introduced to the bath bounce on the bath without coalescence. (Right) A single drop at various stages of a bounce. The droplet size 0.64 mm.

The schematic given in Figure 1 shows the bath being excited vertically. Since the drop is driven by an external excitation from the bath which has two parameters, amplitude and frequency, the drop has the same frequency of the bath (forcing frequency).
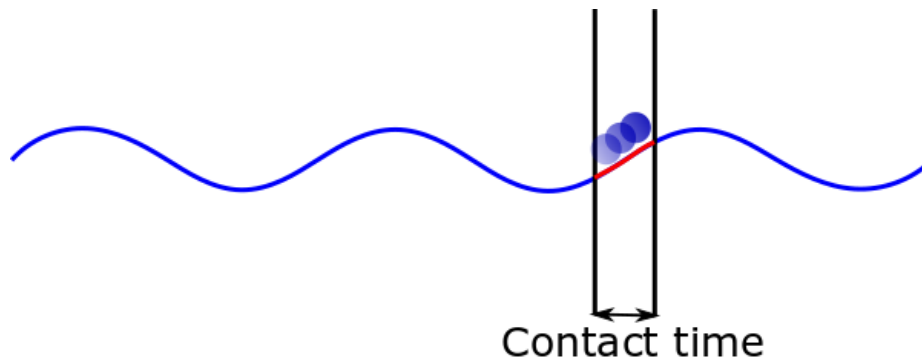

Figure 2: The blue line represents the motion of the surface of the bath w.r.t time and the drop is in close proximity with the bath for the specified contact time.

The drops in our system, come in contact with the surface of the bath and remain in close proximity, till they experience an upward acceleration which is greater than g from the surface. The air layer must withstand the pressure imposed by the drop for the duration that the drop is close to the surface which is illustrated in Figure 2. The upward motion of the bath ensures that the drop stays in contact with the surface up to that point, due to the net effective acceleration pointing downward. Large droplets would require higher acceleration from the bath (more amplitude from the shaker) to leave the surface and small droplets would require a smaller threshold amplitude. The subsequent downward acceleration of the bath gives a net upward acceleration to the drop, propelling it upward with an initial velocity, as illustrated in Figure 3. The equations for the displacement, velocity and acceleration of the bath are given by:

$$d(t) = A\sin(\omega t)$$

$$v(t) = A\omega \cos(\omega t)$$

$$\gamma(t) = -A\omega^2 \sin(\omega t)$$
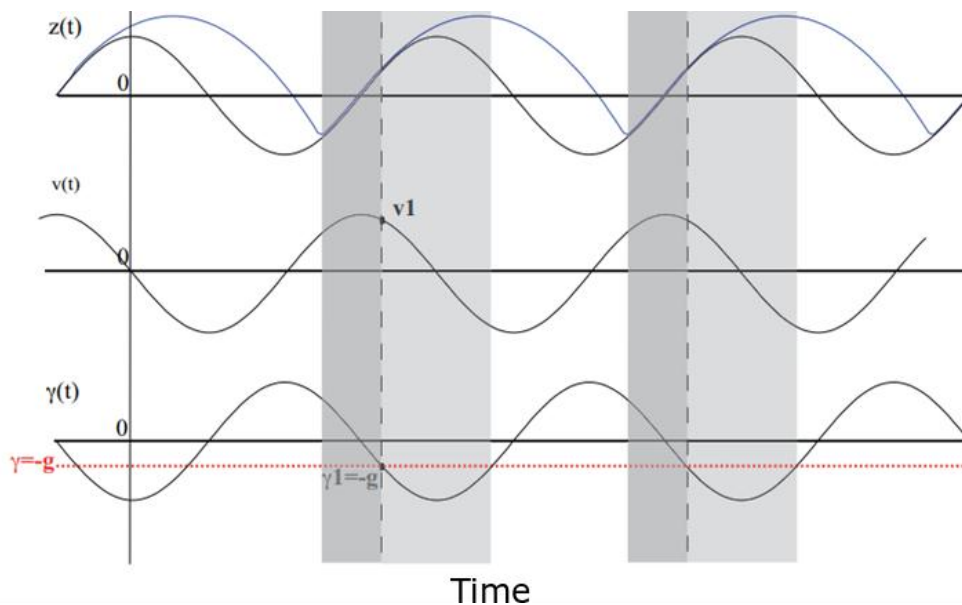
Figure 3 [5]: The functional form of the displacement, velocity and acceleration of the shaker to better illustrate the droplet dynamics. Blue line is the trajectory of the drop. The x-axis is time.

This velocity decides the height and range of the parabolic trajectory of the drop in air. The larger this velocity is, the higher the droplet bounces and longer it takes for the drop to return to the surface. Any drop introduced to the bath below a certain threshold amplitude of the motion of the bath, acquires the same phase w.r.t the bath and w.r.t each other.

1.2 Period doubling of bouncing droplets

One of the interesting aspects of droplet dynamics is the process of period doubling wherein the droplets do a big bounce followed by a small bounce or vice versa. Since this process leads to the possibility of having two stable final states, this is interesting from the point of view of Ising machines. Understanding the mechanism responsible for this would help elucidate and model such a system.

In this section we discuss the process of period doubling for a single drop. Period doubling is brought about by increasing the amplitude of the shaker i.e. increasing the acceleration given to the drop. Upon increasing the amplitude of the shaking of the bath, the contact time of the drop with the surface reduces since it experiences the upward acceleration required to take off more quickly.

Beyond a certain critical point of the amplitude of the shaker, the drop acquires sufficient acceleration from the bath and a large enough initial velocity such that the time it takes to return to the surface is long enough so that the drop lands on the surface while the surface has a net downward acceleration greater than g (the big bounce). This makes the contact time of the drop extremely small since there is a net upward acceleration given to the drop at that point and the drop immediately shoots off the surface. The contact period discussed above refers to the close proximity of the drop with the surface but not in full contact with it (this would result in coalescence). The initial velocity given to the drop at this point is however not as large as the previous bounce. Since, during the big bounce, the drop was propelled with the maximum possible velocity (the bath had maximum upward velocity) as illustrated in Figure 4. So, the droplet does a small bounce with a small height and range and returns to the surface when the surface has a net upward acceleration (the drop experiences a net downward acceleration) and the process repeats. Thus, the bouncing period bifurcates into two bouncing modes. The drop carries out a big bounce followed by a small bounce and this cycle repeats itself. Figure 3 gives an overview of the process.

Upon increasing the amplitude further, the big bounce gets bigger and the small bounce gets smaller. The drops then undergo perfect period doubling [6] where the range of the projectile motion of the drop exactly corresponds to twice the period of the excitation (only one big bounce of twice the period). Till this point, the surface can be essentially treated as flat and to be moving with the base of the bath. Upon further increasing the amplitude, the bouncing period of the drop

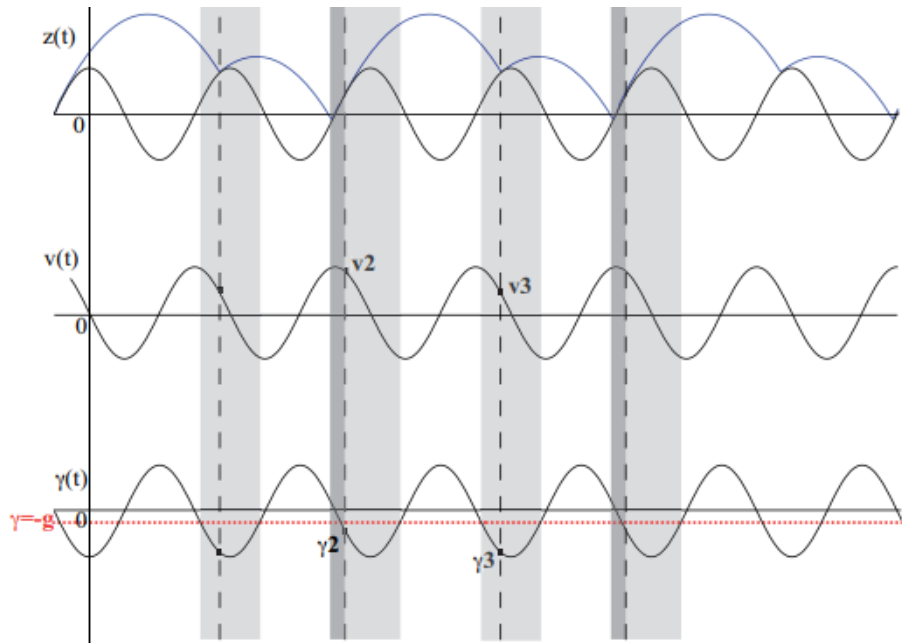*Figure 4 [5]: Functional form of the displacement, velocity and acceleration of the surface as a function of time. The blue line is the trajectory of the drop after period doubling (APD).*

becomes chaotic [5]. The chaotic behavior of the drops is driven by the parametric oscillation of the surface waves and the onset of Faraday instability. Faraday instability can be explained as the formation of surface waves due to increasing the amplitude of forcing, at half the frequency of excitation. All the regimes are represented in Figure 5. Our system lies in the regime of B and a part of PDB. The droplets in our system perform asymmetric bounces.
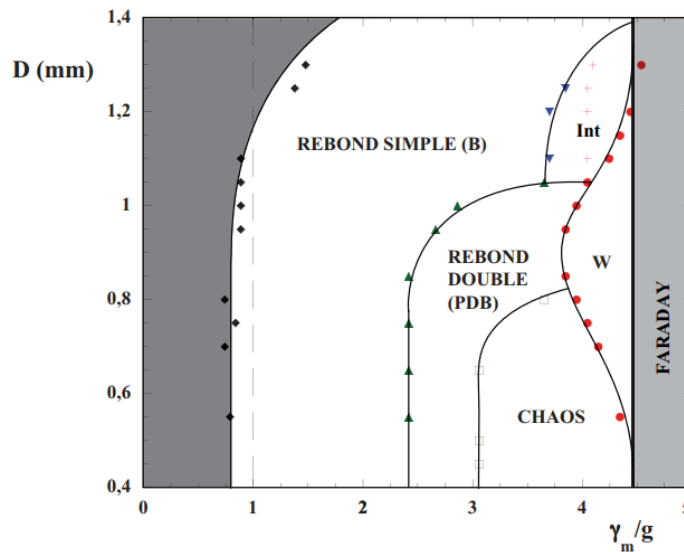

Figure 5 [5]: Different states of a droplet as a function of the acceleration of the bath. The droplets transition from B (Bouncing) to PDB (Period Doubled Bouncing)

1.2.1 Some previous studies

A previous study by [7] has modeled the period doubling with solid boundary conditions and hard spheres exhibits period doubling cascade as given in the figure also by [7].
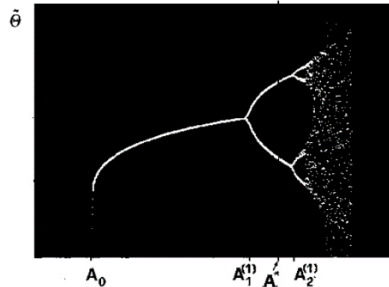

Figure 6 [7]: The jumping particle model exhibits bifurcation in its period followed by a cascade. This is analogous to what happens in our system.

We would expect that the drop inelastically collides with the surface owing to the deformability of both the surface and the drop. This is mostly true however, the contact of the drop with the surface is not a completely inelastic interaction and this would be the case for droplets though the results below 0.6 mm [5]. The surface imparts some part of the energy back to the droplet that the droplet loses during contact and thus the period doubling threshold is actually lower than what can be expected through inelastic collisions. But this difference is extremely small in our case. In our system, we have a lattice of bouncing droplets (more of which will be discussed in the coming sections) which are arranged in different patterns such as in [8].
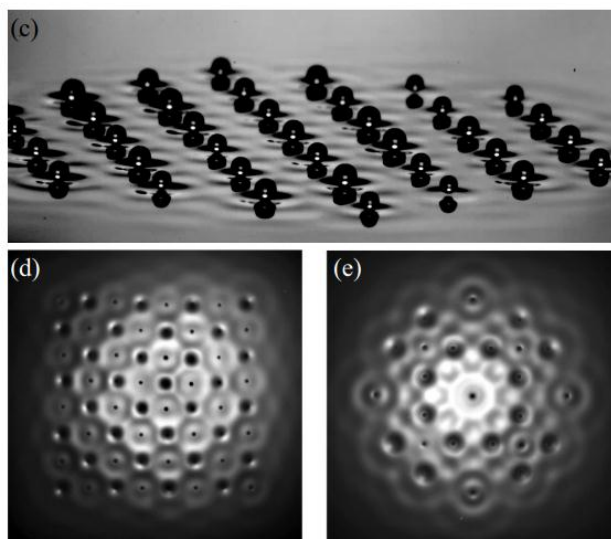

Figure 7 [1]: Lattice of bouncing droplets from [1]. (Top) Side view of the droplets. (Bottom) Different Lattices.

1.3 Our system in the context of the Ising model and Ising machines

The Ising model is used as a computational tool to model materials comprising a lattice of atoms with their magnetic dipole moments of their atomic spins taking the value {+1/-1}. This model is used to study various magnetic phenomena of the comprising material, depending on the description of its Hamiltonian. The most general form of which is the Ising Hamiltonian:

$$H = -\sum_{i.j} I_{i,j}\sigma_i\sigma_j$$

An Ising machine is based on the Ising model wherein materials' properties are simulated using the constituent electron spins as proxies. The Ising machine is such a reprogrammable lattice of 'artificial spins' which have two output values that they can choose from, and they do this selection based on the constraint of having minimum energy since in general, most systems naturally gravitate towards [9] the minimum energy state. Thus, they solve for the ground state of a system.

The motivation behind solving for the ground state is that it represents an optimization problem. The goal of the final orientation of the bi-stable elements in an Ising machine is to obtain a configuration that has minimum energy. For this solution to occur, the system should essentially compute the energy of all possible configurations and acquire the one that has the least energy. This is the definition of a combinatorial optimization problem. Combinatorial optimization problems involve optimizing a quantity from a set of discrete elements. All combinatorial optimization problems can be mathematically mapped [10] to finding the ground state of the Ising Hamiltoian, which is the function of an Ising machine. Combinatorial optimization problems are difficult to solve on a conventional computer since the time required to obtain a solution increases as a power law of the number of elements. Ising machines solve such problems through multiple component interactions which take lesser time than simulating the problem on a conventional computer. Combinatorial optimization problems are NP (non-deterministic polynomial time) hard problems. Np-hard problems are the set of problems that cannot be solved in polynomial time and whose solution cannot be verified in polynomial time. On a conventional computer, problems like multiplication and addition fall under the class of P-Polynomial Time problems with the execution time/complexity scaling as $\mathcal{O}(n^c)$ whereas the set of problems whose execution time scales exponentially (such as $\mathcal{O}(2^n)$), are believed to fall under the set of NP-Non Deterministic

Polynomial Time problems [11]. Thus, the tractability of the solution to the class of NP problems is limited by 'n'. The constraints on designing an Ising machine to solve such problems involve achieving greater freedom in terms of tunability and scaling of the system to involve and allow larger elements that take part in the computation.

Artificial spin systems can be created using systems that have elements with a binary output. Bi-stable systems made of electronic oscillators (like capacitors) were initially used in electronic circuits as logic gates. These elements are called parametrons [12]. The two equally likely outcomes are determined by the noise in the system. They are an example of a system with bi-stable elements. A common recent example of an artificial spin system is the use of Optical parametric oscillators (OPOs). In the case of Ising machines with degenerate OPOs [13], laser pulses are sent through a series of OPOs, which can be programmed to have a Hamiltonian of the desired form and the pulses acquire a phase depending on the said Hamiltonian. The solution to the ground state of the Hamiltonian is the phase configuration of the pulses. OPOs are used to build an architecture capable of solving such problems. Thus, the pulses traverse through the degenerate set of OPOs and acquire a final phase corresponding to the ground state of the system and this phase has a binary output when operating above a certain threshold of the pump field of the lasers. If two pulses are out of phase with each other, the interaction is defined to be antiferromagnetic and if they are in phase, they have a ferromagnetic interaction. Pulses in OPOs represent the elements that need to be optimized and the number of pulses can be scaled [14]. OPOs exploit the fact that the coupling between pulses can be easily manipulated by introducing a suitable delay in the signal. The polarization for lasers [15] is also used in OPOs due to its bi-stable properties (left or right circularly polarized).

In the case of bouncing droplets, upon increasing the amplitude of the shaking of the bath beyond a certain threshold amplitude, the droplets undergo symmetry breaking. Their bounces are no longer consecutively the same. The droplets start doing a big bounce followed by a small bounce or vice versa, see Figure 8. The total time period of the two bounces is twice the original time period. This state is termed as the 'period doubled state' whose process was briefly explained in section 1.2. When this occurs, droplets acquire one of two phases depending on the distance between them. They either start the process of period doubling by doing a big bounce followed by a small bounce or the opposite. Thus, the drops are all in phase w.r.t each other initially and then take up one of

two possible phases. The droplets continuously interact with one another by means of the wavefield they generate on the bath. The droplets take up stable phases which is a function of the interaction between them.

This bi-stable system wherein the elements interact with each other to arrive at a stable configuration corresponding to minimum energy is the very definition of an Ising machine.
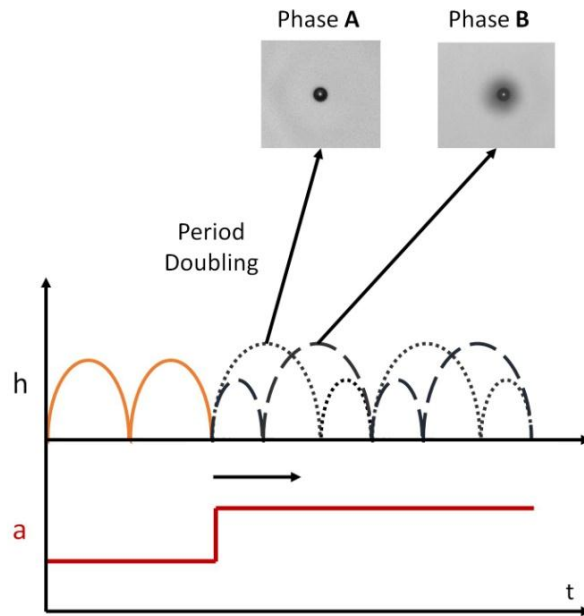
Figure 8 Droplet dynamics as a function of the acceleration of the shaker for the perfectly period doubled case. The amplitude of the shaker (red line) and the trajectory of the drop for BPD (orange) and APD (black). The dotted line represents phase A and the dashed line represents phase B

The images for phase A and phase B in Figure 8 are simultaneous snapshots from the top, of two drops that are out of phase with each other. The gray area around the drop in the snapshot representing phase B, is due to the shadow of the waves created upon close contact of the drop with the surface. The picture depicting phase A on the other hand is devoid of this gray ring around the drop, since the drop is in the air and farthest from the surface, creating no waves. These snapshots in time illustrate the difference in the phase of the bouncing between the two droplets. Any deviation from having a uniform period of bouncing is the onset of the period doubled state.

This bi-stable, macroscopic system has characteristics that are the prominent features of an Ising machine. Thus, this problem is worth exploring in terms of any possible links to the Ising machine, by studying the dynamics of the system.

1.4   Overview

In order to ultimately look at the correspondence of the system with the Ising machine, it is important to probe the dynamics of the droplets. In section 2, we first look at some of the major techniques that were used to acquire information from the system. And this is followed by the process of period doubling of a single drop (section 3.1) and of two drops (section 3.2) in terms of the shaking amplitude of the bath i.e. the acceleration provided to the drops by the shaker. And the simultaneous acquisition of the wavefield of a droplet from the top and its vertical height from the side (section 3.1 and 2.3). And finally, we look at the phase configuration of different arrangements of droplets and different number of droplets (section 3.4). The wavefield envelope of a single drop was also used to simulate the empirical interaction between drops by looking at the decay rate (section 3.1) of the waves produced by a drop. This was used to check if the final phase configuration obtained corresponded to the one with minimum energy. The data obtained from the wavefield was used to simulate the actual Hamiltonian of the system (section 3.3). The outlook of this project involves a precise mapping to the Ising Hamiltonian if possible, and introducing changes to the coupling between droplets to gain a better handle on the interaction term.

If these limitations are solved, we would have a palpable, physical, macroscopic system capable of solving combinatorial optimization problems which could then be mapped to NP-hard problems. This system is currently very much reproducible, adding physical components that are tunable would make the system more versatile in terms of the dynamics. If a mapping to the Ising Hamiltonian is possible, it would mean that the problems that would essentially take more time on conventional computers could be solved by means of a physical system with simultaneous many body interactions. The work carried out here is motivated by that final goal.

Apart from having an interesting potential application, this system has very intriguing aspects in terms of the dynamics of the drops. The full understanding of the dynamics of the droplet is a complex hydrodynamic problem involving dynamical coupling between the surface and the droplets. The interaction between the drops is highly robust and reproducible. The configurations involving many droplets have symmetric solutions. So this system makes for an interesting fluid dynamics and soft matter problem in and off of itself.

2 Experimental Method

In this section we look at some of the techniques and tools to analyse the dynamics of the drops. In section 2.1 we look at the set-up used to perform the experiments, which were all built from scratch. In section 2.2, we look at the droplet generator which was built to produce uniform sized droplets since the drop size plays a major role in the change in the period doubling threshold. In section 2.3 we discuss the technique of wavefield imaging using the schlieren method. In section 2.4 and section 2.5 we look at methods used to track the bath and detect drops respectively.

2.1 Experimental Setup

Silicone oil used for the experiment has a refractive index of 1.4, viscosity of 20×10^{-3} Pa s, density of 0.971 g/ml and a surface tension of $0.021 \, Nm^{-1}$ [1]. The silicone oil bath has a dimension of 10 cm x 10 cm. The silicone oil bath is fixed on the shaker. Shaker specifications: Bruel and Kjaer type 4808. The shaker is connected to the amplifier by Bruel and Kjaer, type 2719. The function generator used to feed signal into the amplifier is by RIGOL DG 1022. The components of the droplet generator are listed in section 2.2.
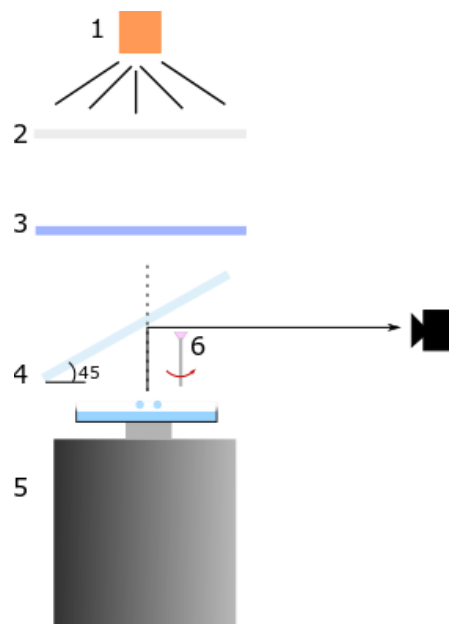

Figure 9: Only the top view of the bath acquired, for observing the final solution of a lattice of drops. (1) Light source, (2) Diffuser for homogenous light, (3) Frenel lens for focusing light, (4) Half-way mirror, (5) Shaker with the bath and (7) Portion of the Droplet generator. Basler camera, 1300-200μm

The first implementation of the set-up given by the schematic in Figure 9, was used to look at the top view of the bath with many droplets, to analyse the phase in terms of the shadow of the waves (gray area tracking). The camera was synchronized with the bath and was used at 400 fps. Since the lighting was from the top, the waves formed from the impact of the drop close to the surface, cast a shadow around the drop which varied in time. This was a good proxy for looking at the transition to period doubling. A half mirror which transmitted half the light and reflected half of it was placed at 45 degrees and used to observe (from the top) the bath. For three drops, the phase

transition was analysed by looking at the shadow of the waves formed by the drops from the top and tracking the change in the area of the shadow. The droplet generator will be discussed in more detail in section 2.2.
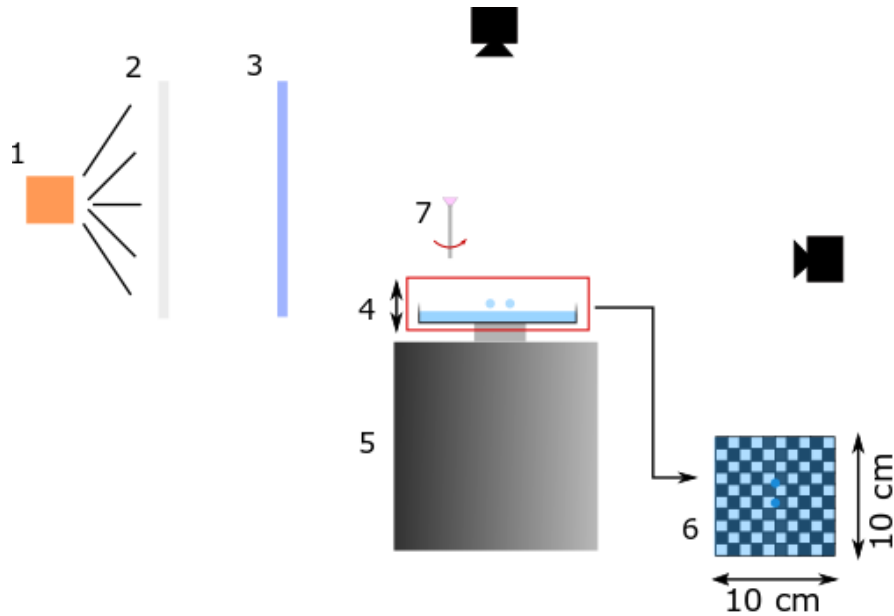

Figure 10: Set-up used for acquiring simultaneous vertical motion and wavefield of the drop. (1) Strong light source, (2) Diffuser to have a homogeneous source of light, (3) Frenel lens for focusing the light onto the surface of the bath, (4) Bath being excited vertically with a dimension of 10 cm x 10 cm and having a checkered grid at the bottom, (5) Shaker for exciting the bath, (6) Checkered grid and (7) portion of the droplet generator.

In a variation to the first set-up, the second set-up was used to simultaneously acquire the wavefield and the vertical motion of the drop. The set-up is illustrated by Figure 10. The bath was lit from the top to observe the distortions of the checkerboard and from the side to observe the vertical motion of the drop. Both the cameras were strobed. They were also synced with each other and with the shaker. Vibration damping material (rubber padding and sponge) was used to isolate the camera on top from the vibrations of the shaker. The checkerboard was printed on an OHB sheet (since paper cannot be used) and the empty squares were painted white to enhance the contrast and reduce reflectivity of the sheet.

2.2   Droplet Generator

In order to ensure that the process of period doubling of the drops is only based on the external excitation (increasing the amplitude of the shaker), we need to produce droplets that are reproducible and of the same size throughout the course of all the experiments. Various methods of conventional droplet generation involve manually producing droplets by using a pick to pinch off drops from the surface and later screening them to select the ones with the required size.

While dispensing drops from a pipe, the diameter of the drops dispensed is a function of surface tension of the fluid and the diameter of the opening. There are two opposing forces i.e. gravity and surface tension. The mass of fluid dispensed is a function of the width of the opening, thus the width becomes a limiting factor for obtaining smaller droplets and it has been a major problem in studying various phenomena which involve producing uniform sized droplets.

The drops formed from a narrow opening under the influence of gravity, are roughly twice the diameter of the opening. Shaking the opening would cause the drops to pinch off for smaller diameters due to the added component of acceleration. We considered options for producing drops using piezo actuators which use the principle of inkjet printers, and in spite of these set-ups requiring a lot of components and automation, they do not perform very well. The nozzles often get clogged and the system has to be operated continuously for a stable output, making it necessary to screen and select drops of the required size.
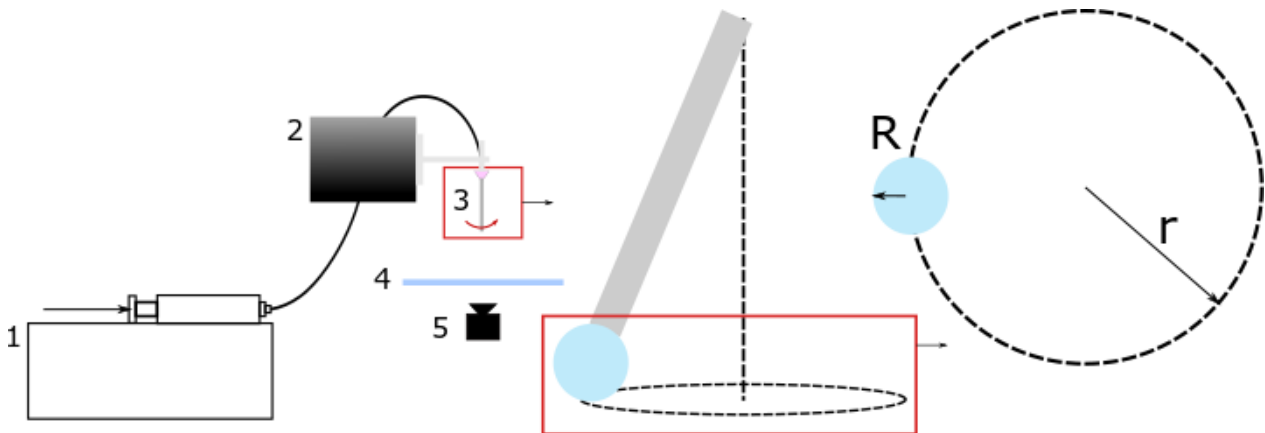

Figure 11: Apparatus for generating droplets. (1) Syringe pump used to pump fluid into the Teflon tip at a constant flow rate, (2) Mini-shaker used to excite the Teflon tip, (3) Teflon tip, (4) Plexi glass to prevent oil from coming in contact with the camera lens, (5) camera.

In order to produce droplets, the basic parameters that need to be addressed are fluid flow control and uniform excitation of the nozzle. So, we decided to build a system comprising these elements. We use a syringe pump to ensure a constant flow rate (7.1 ml/hour) of silicone oil and connect the syringe to a Teflon tip by means of synthetic tubing. The Teflon tip was flexible enough so that the tip could move when connected to a shaker. The Teflon tip performed circular motion because of a slight curvature to the tip. The details of the set-up can be found in Figure 11.

The idea was to operate close to the natural frequency of the tip. The tip performed circular motion (ellipsoidal motion when excited with greater amplitude). The tip ejected two drops in each rotation. One small drop which was not used and one big one which was easily distinguishable from the small ones when observed on the bath, without any microscopic tools or image processing. The size of the droplets in our system is of the order of 0.64 mm, allowing the drop to remain spherical while it performs projectile motion in each bounce, since the capillary pressure supersedes the hydrostatic pressure [3].

2.2.1 Materials

Teflon tip which is used to blow air/dispense fluid on surfaces, model:

Precision Tips Nordson EFD , PN: 7018362, TIP 25 GA PP 0.014 X 1.5'' RED 50P, Lot/SN: 4002264664

Figure 12: Teflon tip of length ~5.8 cm

Mini-Shaker: Bruel and Kjaer, shaker type 4810

Function generator (to produce sinusoidal excitation with tunable frequency): RIGOL DG4162

Amplifier (amplifies the signal from the function generator): KONIG AMP4800

The radius of the drop as a function of the acceleration of the tip was studied.

2.2.2 Method

Assuming that the drop coming out of the Teflon tip is roughly spherical. The tip is being rotated at a constant angular frequency 'Ω'. The surface tension of the fluid is 'μ'. The mass of the drop is 'M' and the radius is 'R'.

Thus, equating the centrifugal and surface tension forces we have:

$$M\Omega^2 r = 2\pi\mu d$$

$$M = \frac{\mu R}{\Omega^2 r}$$

$$\frac{4\pi R^3 \rho}{3} = \frac{2\pi\mu d}{\Omega^2 r}$$

$$Thus, R^3 = \frac{k}{\Omega^2 r}$$

$$where\ k = \frac{3\mu d}{2\rho}$$

$R_0 = \left(\frac{\mu d}{\rho g}\right)^{0.5}$ R_0 is the radius of the drop in the absence of the circular motion.

$$Thus, we\ expect\ a\ linear\ relationship\ between\ R^3\ and\ \frac{1}{\Omega^2 r}.$$

Table 1: Mean values of the angular acceleration, radial distance from the center of suspension of the tip, centrifugal acceleration, radius of drop, and cube of the radius of the drop.

Ω (Hz)	r (mm)	$\Omega^2 r$ (mm/s²)	R (mm)	R³ (mm³)
566.5121	0.0624	20026.40387	0.3458	0.04134994791
554.3954	0.1325	40724.43939	0.3194	0.03258402538
546.36	0.2497	74537.75963	0.2735	0.02045841538
546.36	0.4027	120209.6748	0.2431	0.01436662899

The data fit given in Figure 13 has an R squared value of 0.9394. The red box is the condition set implemented for the subsequent experiments involving droplets.

The standard deviation of the distribution as shown in Figure 14 is very small, with a range of [0.469 mm, 0.4924 mm, purple] , [0.533 mm, 0.5568 mm, yellow], [0.625 mm, 0.6455 mm, orange] and [0.672 mm, 0.6994 mm, blue] with a standard error of (purple, 0.092 %) , (yellow, 0.118 %) , (orange, 0.0461 %) and (blue, 0.086 %). In the configuration that we use, with 40.72 m/s² acceleration the standard error is the least i.e. 0.05 %. Thus, our droplets are of the size 0.6387 mm +/- 0.0006 mm.
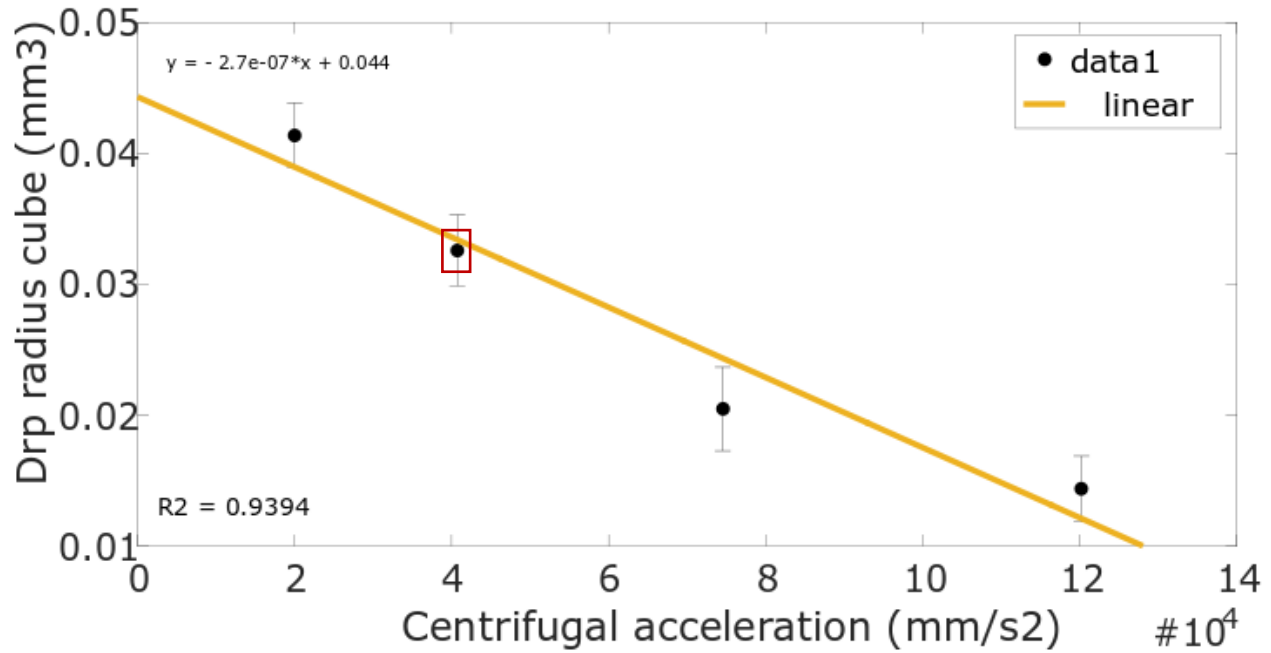
Figure 13: A linear fit between the mean radius cube and the mean centrifugal acceleration for each of the cases (4 points) was done.
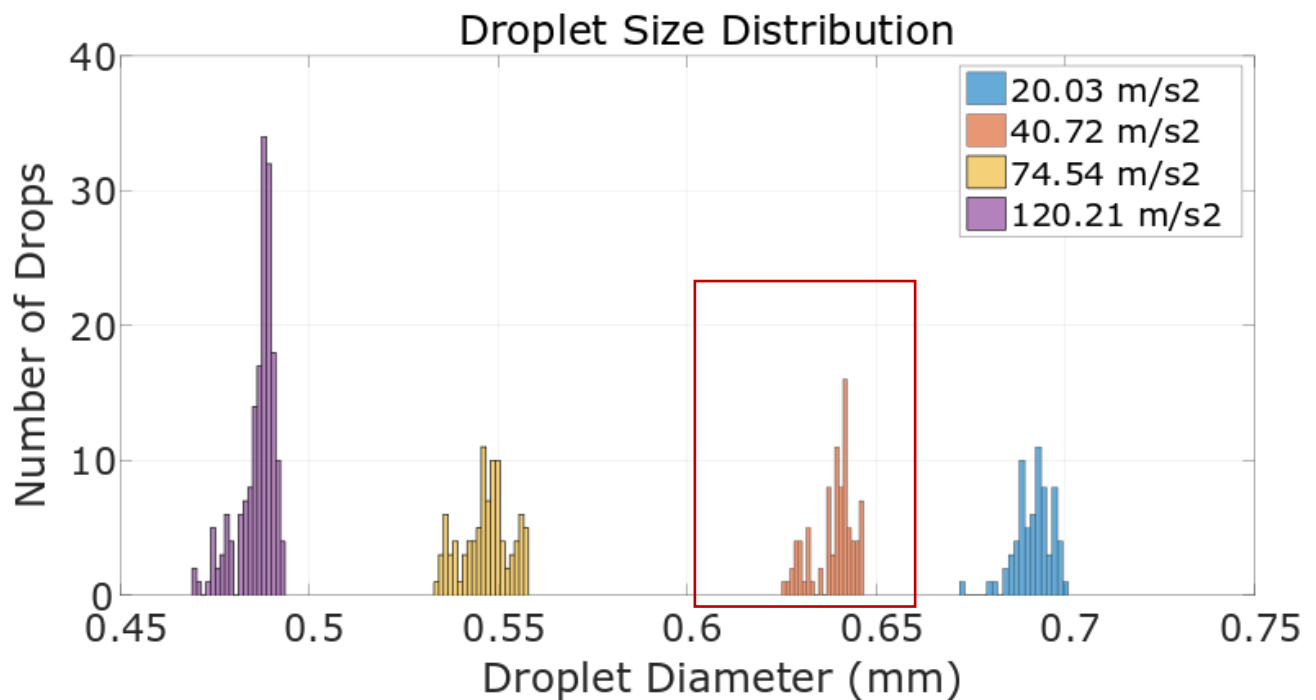

Figure 14: The distribution in the size of droplets as a function of the acceleration experienced by them. The total number of droplets sampled for each of the cases was different since the total recorded frames was the constant parameter. The number of drops are as follows: purple (120.21 m/s², 174 drops), yellow (74.54 m/s², 96 drops), orange (40.72 m/s², 87 drops) and blue (20.03 m/s², 68 drops).

2.3 Wavefield Imaging

The interaction of the droplets is mediated through the wavefield between them. The wave interaction between the droplets is a key component in understanding the dynamics of the system. The wavefield was imaged using the schlieren technique by means of the demodulation of a checkered backdrop [16]. A light beam that enters the surface appears to from point A due to the slope at the surface. The actual location of the beam being point B, as represented in Figure 15 whose would look like Figure 19. This displacement vector can be calculated using small angle approximation. The same process occurs in y direction as well.
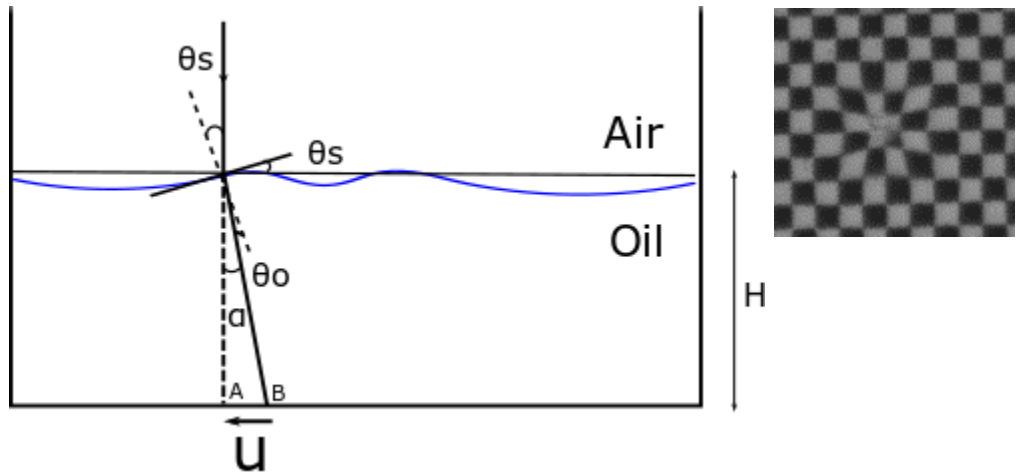

Figure 15: Schematic of a wave (exaggerated) on the surface of the bath. Light rays are incident at theta s on the surface and get refracted at alpha. The grid is at the base of the bath. The points on the grid appear to come from point A, but are actually from point A, but are actually from point B. Inset on the right is the top view of the actual experimental distortion of the grid due to impingement of the drop.

Small angle approximation can be used since all the displacements are very small.

$$\vec{u} = -\alpha H$$

$$\alpha = \theta_s - \theta_0, \theta_s \text{ has to be calculated}$$

$$Snell's law: n_0\theta_0 = n_a\theta_s$$

$$\theta_0 = \frac{n_a\theta_s}{n_0}$$

$$\alpha = \theta_s - \frac{n_a\theta_s}{n_0} = -\theta_s\left(1 - \frac{n_a}{n_0}\right)$$

28

$$\vec{u} = -\theta_s \left(1 - \frac{n_a}{n_0}\right) H$$

$$\theta_s = \frac{dh}{dx} \quad (slope\ of\ the\ wave),\ similarly\ \vec{u}\ along\ y\ direction.$$

$$\vec{u}_{pxl^2} = -\left(1 - \frac{n_a}{n_0}\right) H_{pxl} \nabla h_{pxl}$$

$$\nabla h_{pxl} = \frac{\vec{u}_{pxl^2}}{\left(\frac{n_a}{n_0} - 1\right) H}$$

$$h = -\int_0^x \nabla h_{pxl} . \vec{dl} = \frac{1}{\left(1 - \frac{n_a}{n_0}\right) H} \left(\frac{pxl}{mm}\right)^2 \quad and\ n_a = 1.0029, n_0 = 1.4,$$

$$H \sim 15mm\ (measured\ precisely\ for\ each\ experiment)$$

The resolution in x and y directions being of the order of 0.04 mm. The height is limited by the precision of height measurement of the bath which is measured by a screw gauge with a least count of 0.01m. The height was measured 5 times repeatedly for each experiment and the standard deviation was used to compute the precision which was of the order of 0.01 mm.

The detection of the wavefield very close to the drop (~0.5 mm) is not very reliable due to the large distortions of the checkerboard/black and white grid. The grid size must be larger than the wavelength of the waves that are to be observed. The distortions of the grid must be small enough to be able to look at the dominant peaks in the Fourier space in the vicinity, without having them blow up to infinities. This can be achieved by using a larger grid size for the checkered backdrop, but this would cause a dip in the height field resolution. Thus, various grid sizes were tried, to optimize this trade off and a grid of 0.5 mm was chosen to visualize the wavefield. The wavefield was captured by the method of strobing the camera to increase the effective frame rate. Droplets bounce at 80 Hz on the surface of the bath. One bounce takes 0.0125 s, which would mean that we would require a frame rate of 800 Hz to obtain ten points of the droplet's trajectory in one bounce. More points for greater temporal and spatial resolution would mean increasing the frame rate of our camera. This would have restricted the field of view and result in loss of some waves.

In order to circumvent this issue of having to increase the frame rate of the camera, a strobing technique was used. Instead of having the frame rate of the camera correspond to a multiple of the bouncing (for both BPD and APD) the camera was strobed at slightly below the frequency of the bouncing of the drops. Since the lower frequency is the APD state i.e. 40 Hz, this was chosen as the upper limit. (BPD-before period doubling state and APD-after period doubling state)

*Figure 16: Bounces at time of period T. Camera strobed at T-t.*

$$The\ required\ condition\ is\colon n(T-t) = (n+1)T$$

$\dfrac{1}{T-t}$ *is the FPS of the camera and* $\dfrac{1}{T}$ *is the frequency of bouncing taken to be* $40Hz$.

$$\frac{1}{T-t} = \frac{n}{(n+1)T}\ if\ n = 39\ and\ T = 0.025\ s, then\ \frac{1}{T-t} = 39\ Hz.$$

Thus, at 39 Hz and 156 total frames, 8 cycles (BPD) and 4 cycles (APD) of the bouncing dynamics was recorded. This encapsulated 39 points in one bounce. The wavefield was captured for 13 different amplitudes of the shaker. The simultaneous imaging of the side view was carried out to probe the relation between the wavefield and the process of period doubling. The transition to period doubling was observed by looking at the variation in the time taken to complete one bounce by the drop.

2.4   Tracking the vertical height of the drop
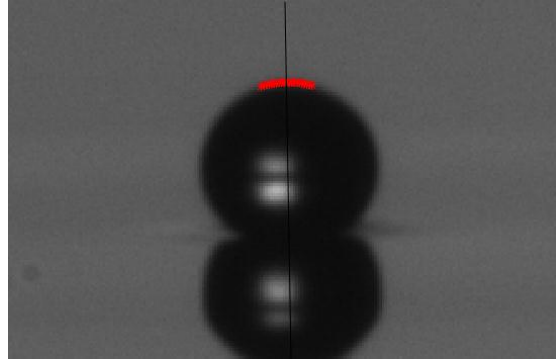
Figure 17: Black Line-Column of pixels with the top most part of the drop. Red dots-sub-pixel detection of droplet edge. Step1: pixel detection of topmost point of drop Step2: column of pixels of topmost part of the drop detected through convolution. Step3: On adjacent columns on either side of the above column, the droplet detected again using convolution. Step3: Fitting parabola to the detected drop edge at taking point of maxima as the position of the drop.

For the vertical motion of the drop, the drop was initially detected with pixel precision using thresholding which was then followed by detection using convolution. A column of pixels passing through the topmost part of the drop was selected (represented by the black line passing through the drop in Figure 17) and this column was convoluted with the function $[\sigma^2 * column\ of\ pxls *$ $e^{-(column\ of\ pxls/\sigma)^2/2}]$ where σ is a small number (point spread), to obtain the dip in intensity which is apparent when we encounter the top of the drop (since the drop is black and the background is gray). This allowed for detection with sub-pixel accuracy. This process was repeated to pixel columns adjacent to the top most point of the drop and a parabola was fit to around 10 such columns on either side of the column of pixels containing the top most portion of the drop. This fit was also in sub-pixel range. If one pixel measured about 0.04 mm, doing sub-pixel detection would give a precision of the order of 0.001 mm (measured from the standard deviation of the fit). The maxima of the parabola was considered as the drop location. The top of the drop was not affected by the process of impingement and is a less noisy surface compared to the bottom. Thus, tracking the droplet's center was not carried out.

2.5   Tracking the excitation of the bath
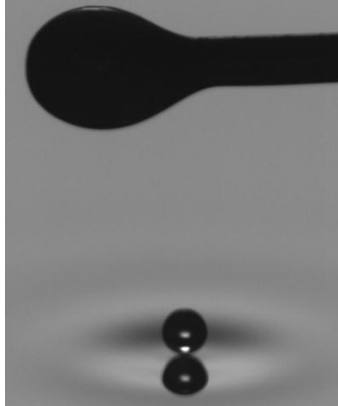
Figure 18: A drop with the needle (top) as a proxy for the position of the shaker.

The bath was made to move sinusoidally with a given frequency and amplitude. In order to look at the real time displacement of the bath, a proxy was used (needle with rounded end, refer Figure 18) to track the displacement of the bath. A thin needle with a spherical head was attached to the side of the bath that moved in consonance with the bath, allowing us to gain information on the actual displacement of the bath. The needle was again detected using the same method used for the drop to gain sub-pixel accuracy for bath displacement. This was plotted alongside the droplet trajectory to reproduce the predicted motion of the two (Figure 20).

Thus, the temporal resolution obtained was, 0.0001 s and the spatial resolution for the vertical motion of the drop was in sub-pixels with up to 0.001 mm and for the wavefield the height accuracy was 0.01 mm with an axial resolution of 0.04 mm.

3   Results and Discussion

In this section we discuss the results of the project. We start with the case of dynamics of a single droplet in section 3.1. Simultaneous acquisition of the wavefield, the vertical motion of the bath and the droplet's vertical motion has never been done before, and has been carried out here. The data obtained could help model the entire system and all its dynamics, in the future. Section 3.1 also covers the process of detecting the bouncing period. The wavefield obtained in section 3.1 was also used to simulate an Ising type model of the system (section 3.3) and look at the degree and strength of interaction. The dynamics of two droplets is studied in section 3.2 which gives an insight into the interaction. Different lattices of droplets were studied (section 3.4) and their solutions corroborated with the simulation in section 3.3. Finally, some preliminary experiments on moving droplets to unstable positions were carried out in section 3.5.

3.1 Period doubling of a single drop
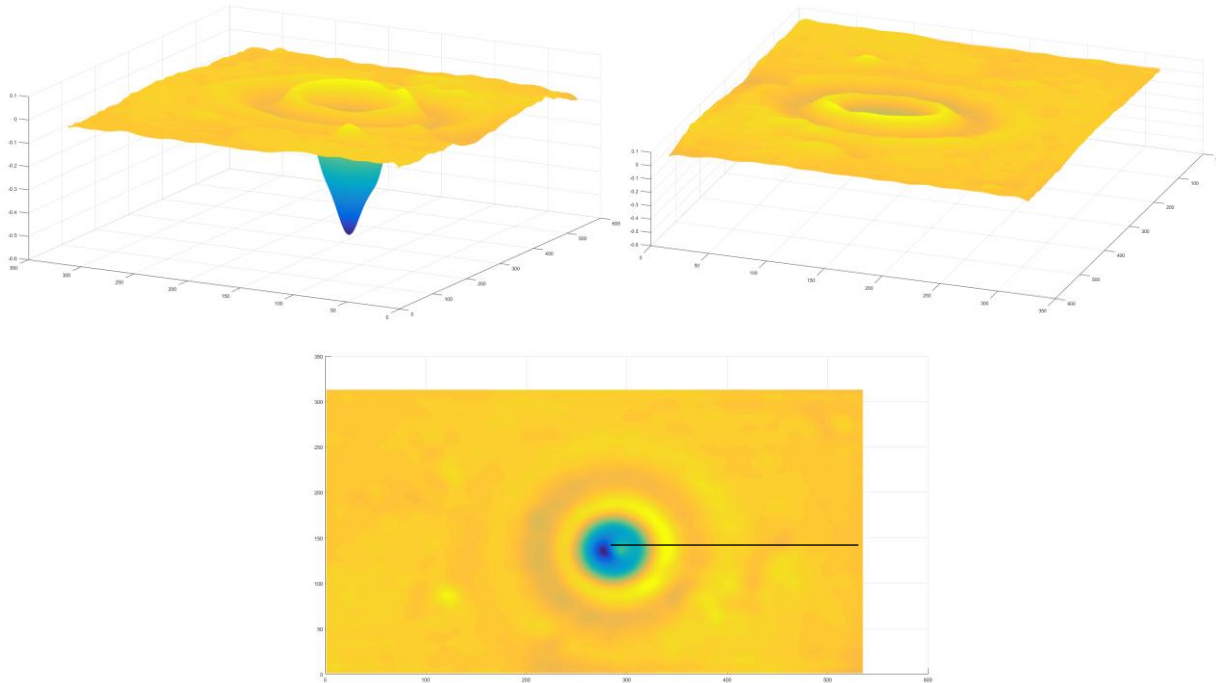
Figure 19: Wavefield image of a frame, 3D plot at different viewing angles. (Top, Left) Includes dip in the surface (blue) that the drop creates upon impingement. (Top, Right) Wavefield around the impingement. (Below) Top view of the wavefield.

The wavefield imaging for one frame of the bounce is given in Figure 19. The wavefield was measured using the technique described in section 2.3. The radial average of the wavefield was used to track the wave front in time. The black line in Figure 19 (bottom), represents the direction in which the radial averaging was carried out.

The dynamics of bouncing droplets with the surface was experimentally reproduced from [5] as shown in Figure 20 (bottom). The droplets are in contact with the surface till they are given a net upward acceleration by the bath, at which point they shoot off the surface. This is followed by a projectile motion of the droplet and the drop lands on the surface again to repeat the process.

The key feature of this analysis is to look at the variation of the time taken for consecutive bounces. This contains the information on period doubling. The wavefield for the drop was also simultaneous analysed. These quantifications have not been done previously.
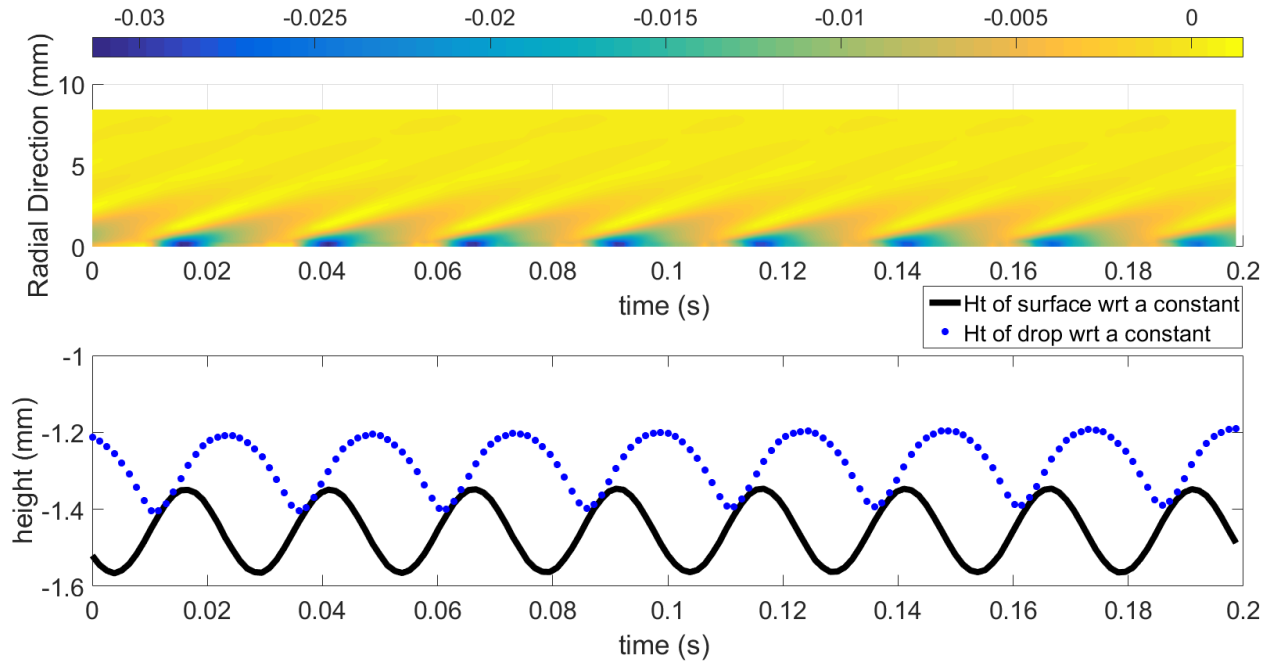
Figure 20: BPD state- (Top) The wavefield of the drop as a function of time. The colour scale gives the depth of a row of pixels, radially outward from the drop. (Bottom) The vertical motion of the drop (blue, dotted line) and the vertical movement of the bath (black, solid line), plotted together.

In Figure 20 (top), the wavefield is radially averaged and plotted in time. This gives information on the time evolution of the wave front. For a single drop, the process of period doubling is solely driven by the amplitude of excitation of the shaker. The wavefield and the vertical motion of the drops were simultaneously studied to look at the relation between the two. As can be seen in Figure 20 (bottom), the point of contact of the drop with the surface is followed by the generation of the dip in the surface height (blue regions, top) at that point. The droplets also undergo the dynamics with the surface as predicted [5]. Figure 20 (bottom plot) shows the movement of the drop. The displacement of the bath was used to calculate the acceleration experienced by the drop $[(2\pi f)^2 x]$.

We can see that the waves travel in time. The wavefield becomes relevant when we have two or more droplets interacting with one another. The wavefield of a single droplet contains all the information needed to look at the interaction between droplets and analyse the process of period doubling. And the wavefield along with its phase with respect to the excitation (acceleration of the bath) are critical to understanding the evolution of the phase of the droplets after period doubling. Thus, the wavefield and the vertical motion of the droplet and shaker were analysed for thirteen different amplitudes of the shaker, starting from the before period doubled state.

The contact time of the drop with the bath is 0.0026 s. the droplet performs reproducible bounces. This acquisition was over four seconds at the frame rate of 39 Hz. Thus, the dynamics have been completely reproduced and now quantified. The period for the drop is 0.0125 s. The same process was carried out for other cases of amplitude as well.
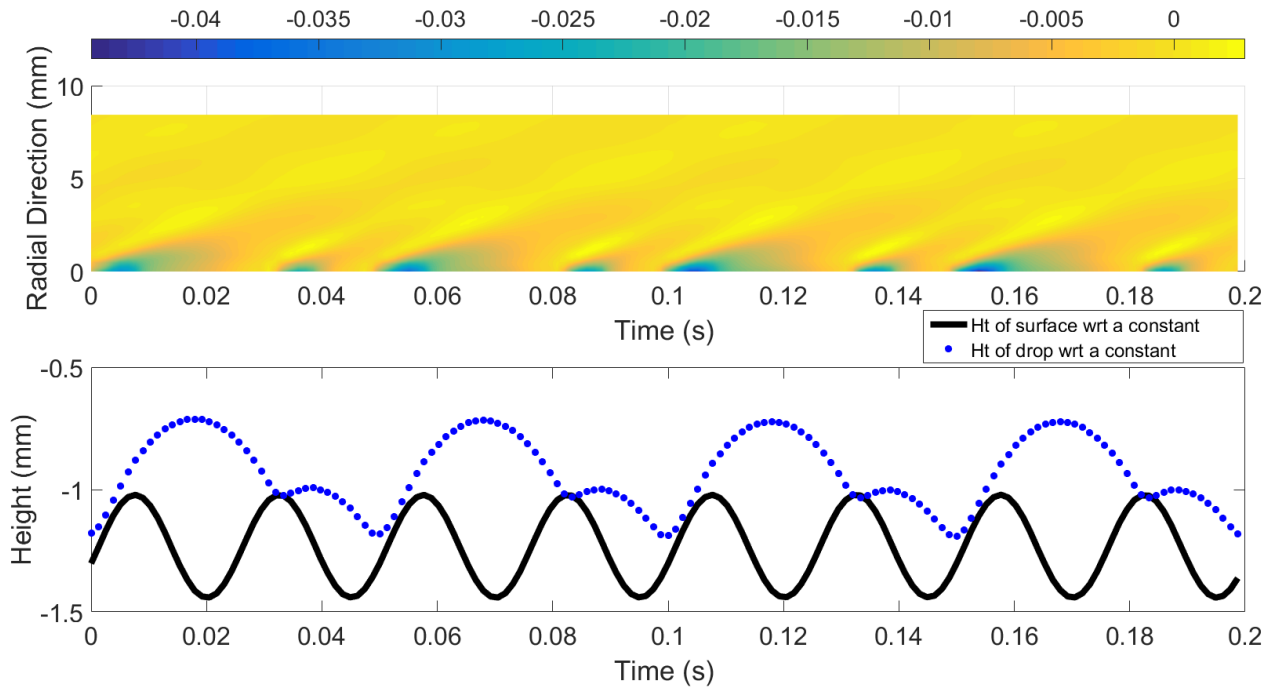

Figure 21: APD state- (Top) The wavefield of the drop as a function of time. The colourscale gives the depth of a row of pixels, radially outward from the drop. (Bottom) The vertical motion of the drop (blue, dotted line) and the vertical movement of the bath (black, solid line), plotted together.

For the after period doubled case in Figure 21 (bottom), we have the droplet doing a big bounce and a small bounce consecutively. For the big bounce, the drop is lifted off the bath when the net acceleration is upward and the velocity imparted is the highest. And at this point, it has sufficient energy to have a longer range along its parabolic trajectory due to higher initial velocity. So the drop comes in contact with the bath at a point in time when the net acceleration (bath + gravity) experienced by the drop points downward. The whole cycle has a period of 0.0250 s which is double the period of a drop in its non period doubled state. The contact time after the small bounce is 0.0045 s and after the big bounce is 0.0012 s. the contact time for the before period doubled case is 0.0026 s. The trends in contact time agree with the expected dynamics.

In Figure 21 (top), the wavefield of the drop is given. It has a very discernable change when compared to the non-period doubled plot in Figure 20 (top). The drop sends out stronger waves when it impinges on the surface after the big bounce when compared to the waves after a small bounce. The waves from the big bounce propagate for a longer period of time as expected.

To trace the process of period doubling, it is crucial to employ detection with high resolution since the order of change in the period is 0.001 s. The droplet position was detected with sub-pixel accuracy as discussed in section 2.4 and the motion of the drop was used to find the time period of each drop, again in the order of sub-pixels. This analysis was done by fitting parabolas to the 11 topmost points (refer Figure 22) of every bounce and finding the intersection of theses parabolas. Since the drops perform projectile motion, the intersection of each of the parabolas would correspond to the point in time which marks the end of one bounce and beginning of the next. The bounce time was given by the difference between these points. This reinforced sub-pixel accuracy of the detections since the fitting was carried out with sub-pixel accuracy. This was repeated for all experiments. The inset in Figure 22 gives the trajectory of the drop as a function of time, with a parabola fit to its top few points.
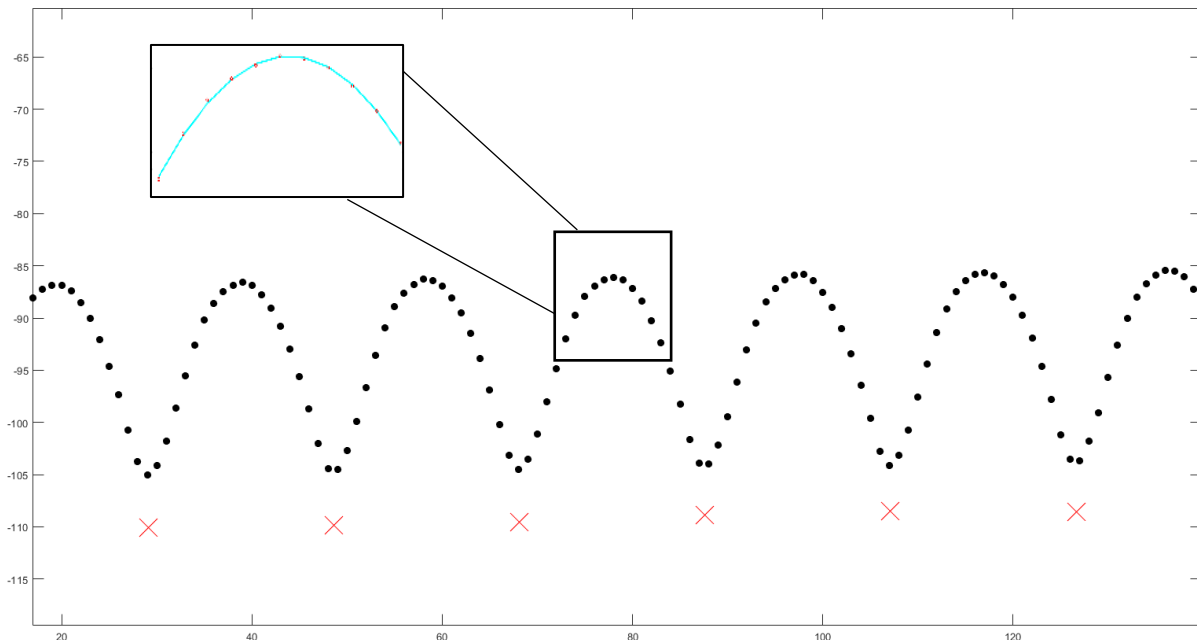

Figure 22: Multiple bounces and the position of the drop (black dots) as a function of time. The point of intersection of the parabola fits (red x) gives the point in time when the bounce is completed. Y-axis is the vertical height and the x-axis is time. Inset contains the parabola fit to the top few points of the trajectory.
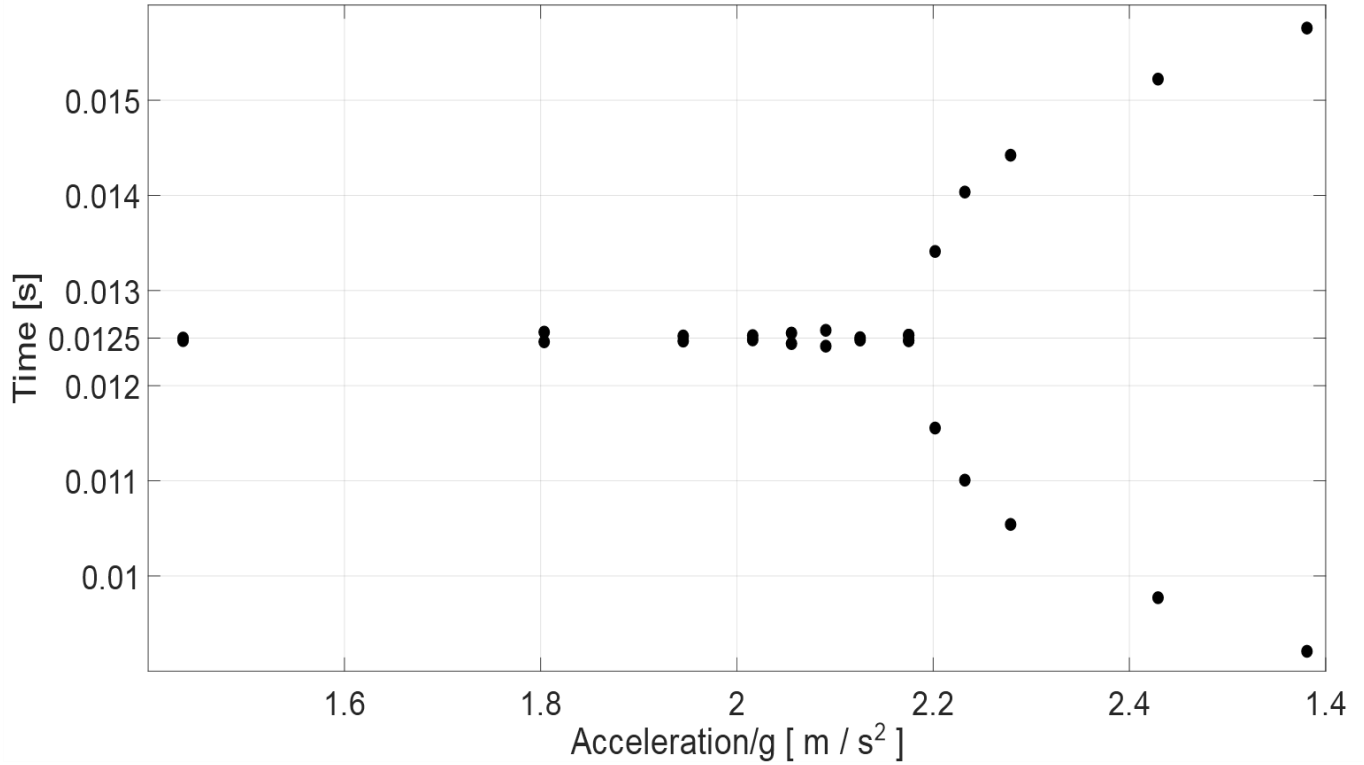
Figure 23: The time between consecutive bounces plotted as a function of increasing γ: the maximum acceleration provided by the shaker.

As we increase γ, the droplets undergo symmetry breaking and the consecutive bouncing period steadily diverges. These experiments also give an estimate on the error of measurement based on the time taken for bounces before the period doubling threshold. Which gives an uncertainty of 0.00001 s. The critical acceleration for symmetry breaking is ~2.9g. These measurements were carried out using the strobed technique to increase the effective frame rate of the camera.

Figure 23 represents the variation in the time taken for each bounce. The period for bouncing bifurcates into two values from (0.01250+/-0.00001) s to (0.01577 +/- 0.00001) s and (0.00921+/-0.00001) s. This data can be analysed in Fourier space for the dominant frequency responsible for the process of period doubling.

These results pave way for modeling the interaction between two drops (superposition of the wavefields of single drops). They contain the phase between the surface and the wave fronts (all wave fronts). All possible variables have been measured.

The wave envelope for all the 13 states was obtained by looking at the depth of the surface across all forty frames. For each point in the radial direction, the minimum negative displacement (maximum downward displacement) was subtracted from the maximum positive displacement of the surface.
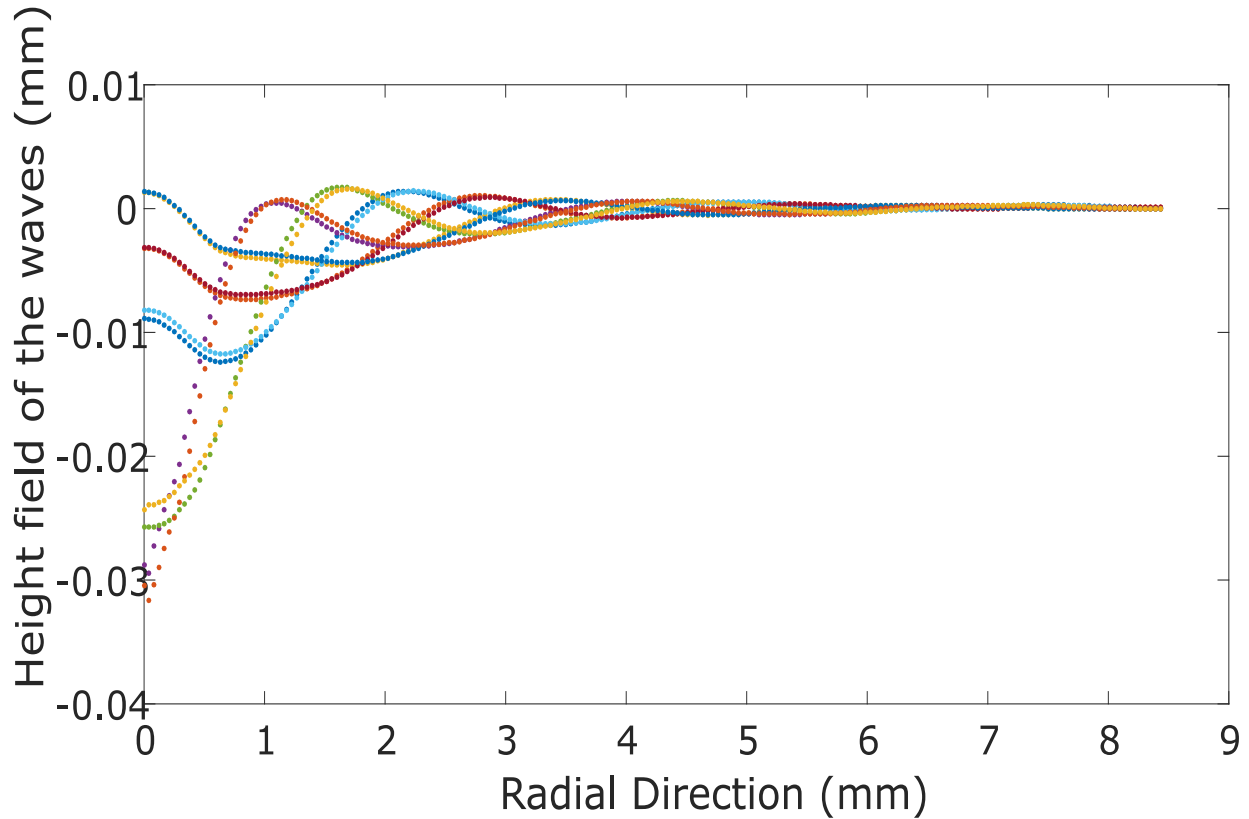

Figure 24: Ten wavefield profiles generated by the drop in time, plotted in one plot to illustrate the general trend. A total of 30 fields in time were used in the fit (spanning one bounce).

The wave envelope obtained in Figure 25 gives information on the rate of decay of waves with distance. The fit obtained (Figure 25) was in close agreement with the proposed functional form of the wave envelope. This was used for the simulation of interaction between droplets in section 3.3.

The coefficients are given by 0.02 mm for *a* and 0.43 for *b*. the equation is given by,

$$f(r) = \left(\frac{a}{\sqrt{r}}\right)(e^{-br})$$

This wave envelope accurately predicts the phase outcome of different arrangement of drops which is elaborated in section 3.4.
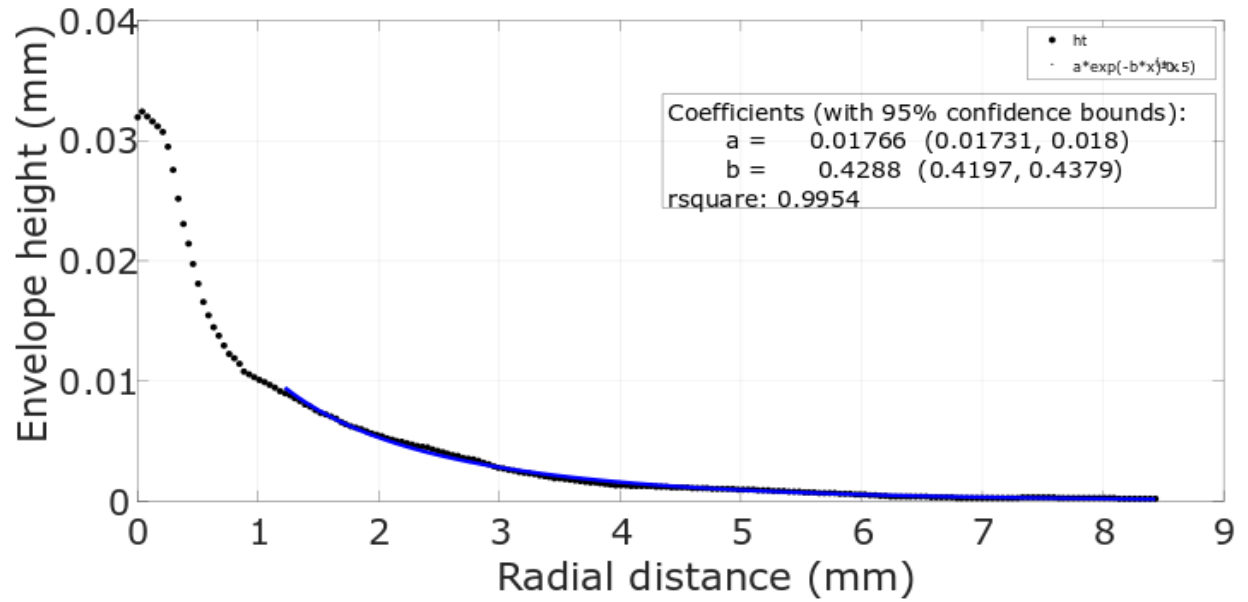
Figure 25: BPD state- The wave envelope across two bounces of the drop before period doubling.
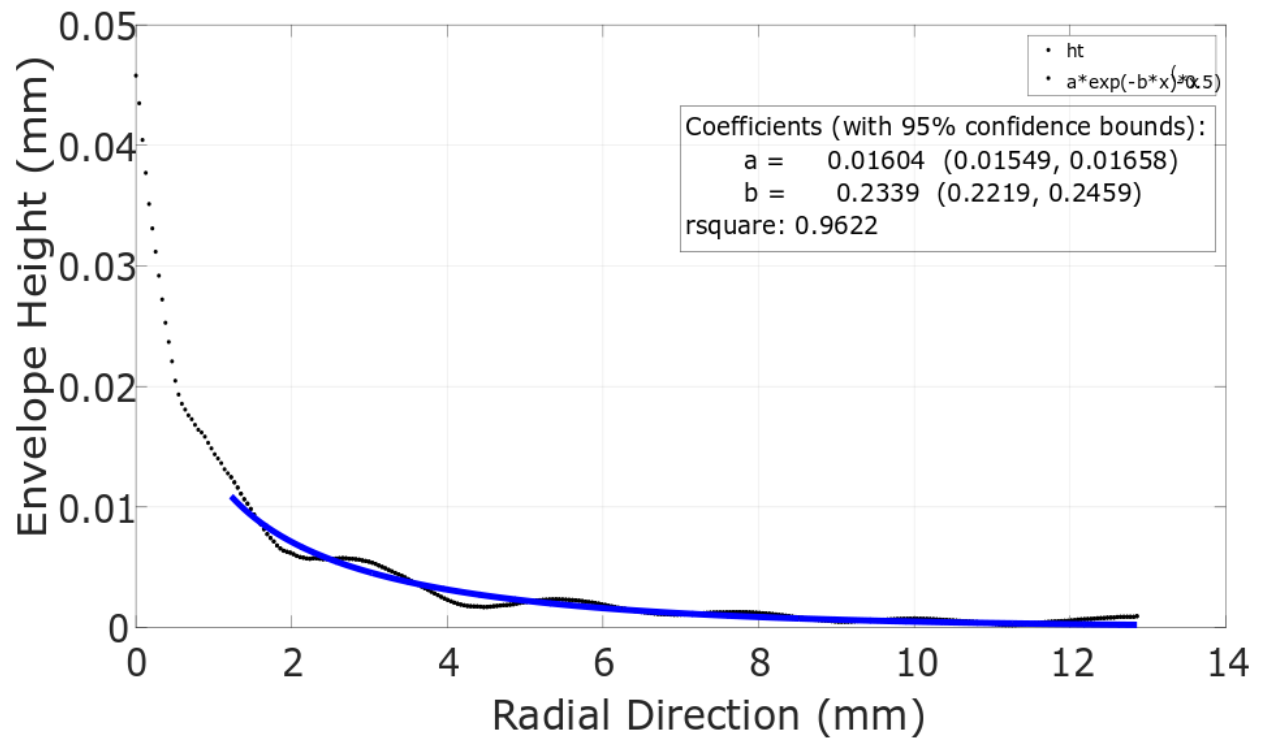

Figure 26: APD state- The wave envelope across two bounces of the drop after period doubling.

The wave envelope starts having some oscillations in the period doubled state in Figure 26 due to the asymmetry in bouncing pattern.
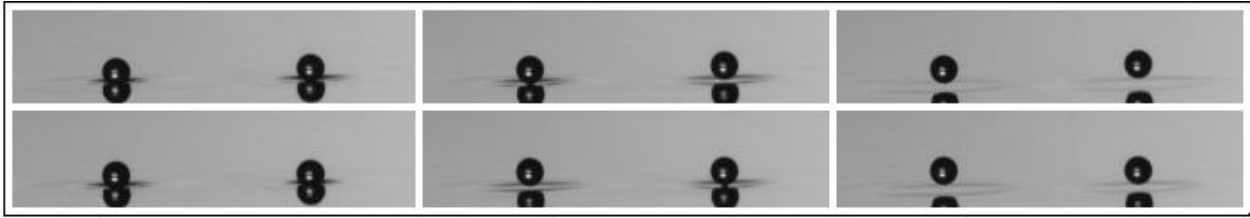
3.2   Phase locking between two drops

Figure 27: Sequence of images for two drops (of size 0.64 mm) bouncing out of phase with each other.
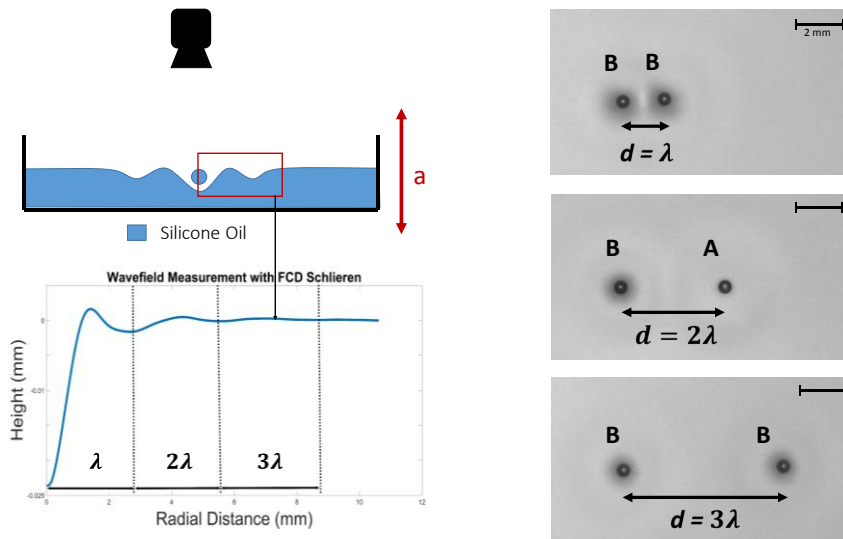

Figure 28: (Left) Wavefield produced on the surface of the bath by the impact of a drop on the surface. The stable positions being roughly equal, stated as λ. The droplets have three natural stable positions that they move to. (Right) Snapshot of drops in phase (top and bottom) and out of phase (middle). The gray area is the shadow of the waves formed by the impact of the drop. When the drop is at its highest point or descending, the shadow is absent since the waves die down. These distances decide the phase of the drop i.e. phase A or phase B.

The stable distances for 2 droplets are:

λ = 2.013 mm , 2λ = 4.99 mm and 3λ = 7.792 mm

Two drops can be easily arranged in one of the three distances represented in Figure 28 (right) when they are successively brought close to one another. These distances are stable because of the absence of longitudinal forces along the surface. The experimental results show that when they are at λ or 3λ the droplets period double in phase, thus the interaction is defined to be ferromagnetic. At 2λ the droplets go out of phase when they period double and the interaction is termed antiferromagnetic.

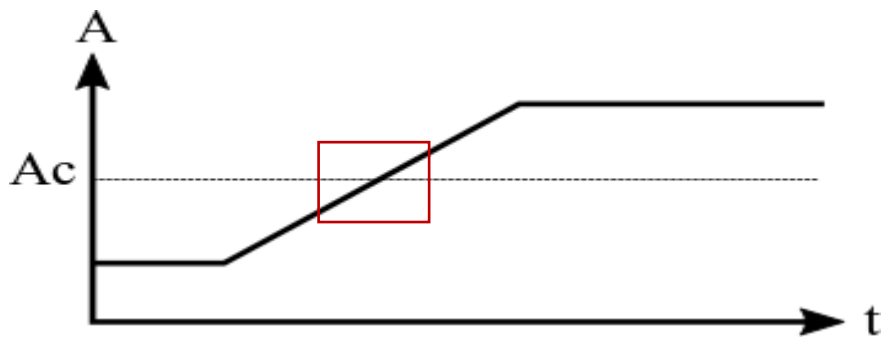When we increase the amplitude as a ramp function of the form:

Figure 29: Amplitude of the shaker 'A' as a function of time. The red box is the region in time that has been zoomed into, in Figure 30.
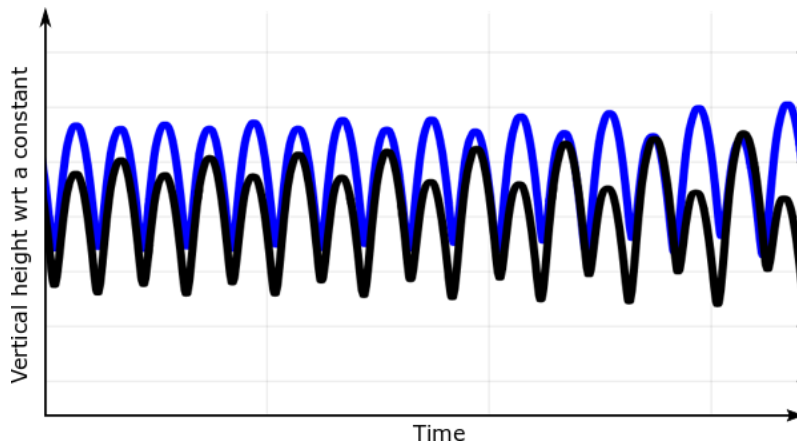
Figure 30: Two drops, drop 1-black and drop 2-blue going out of phase with each other as they transition to period doubling. The amplitude of the shaker is increased by a ramp function.

The slope of the ramp function as it becomes more flat/reduces, does not allow for mistakes, but an interesting case occurs when the slope is sufficiently large to provoke a miscalculation by the dropletsm followed by a correction by the system by virtue of mutual interaction.
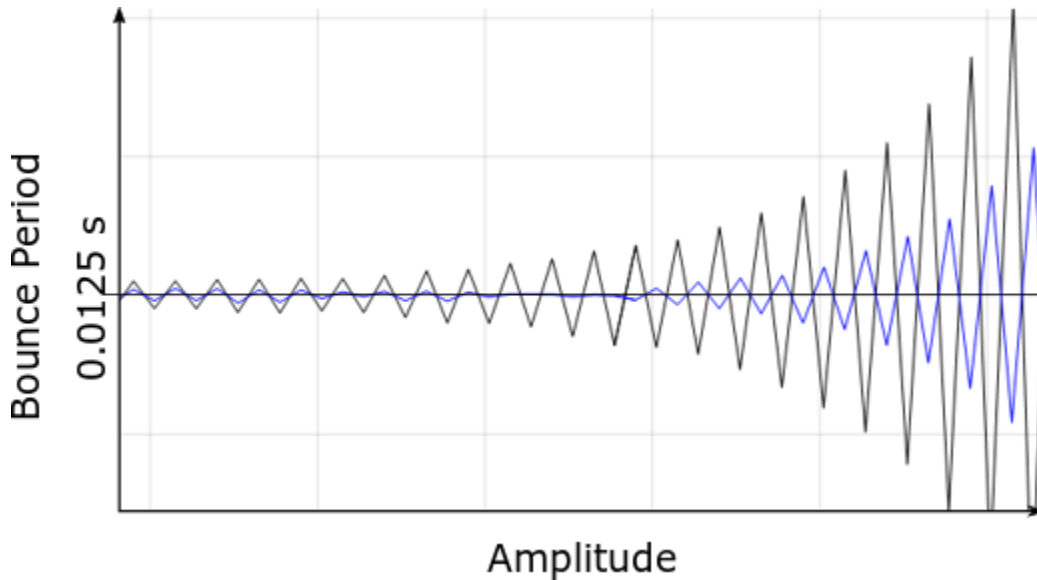
Figure 31: Zoomed in portion of Drop 1 –black, period doubles first followed by drop 2-blue, under the influence of a linearly increasing amplitude. The second drop (blue) stops being period doubled due to feedback from Drop 1. The x-axis is amplitude and the y-axis is the time between consecutive bounces.

In Figure 31, the deviation in time period is represented by connected lines to illustrate the oscillatory behavior of the droplets performing a big bounce followed by a small bounce. In the case of two droplets as depicted in Figure 31, the first droplet (black) period doubles, and the second droplet (blue) follows suit with the same phase, but the droplets interact with each other and the second drop (blue) flips its phase after which point the asymmetry in the consecutive time period grows with the amplitude. This experiment establishes the fact that (a) the interaction between the droplets is strong enough at 2λ to flip the phases and (b) the droplets are actively calculating the net energy by constantly interacting with one another (c) the growth of stable modes can occur at slow rates of change in amplitude and (d) the rapid growth of asymmetry between the two droplets' periods at a given time once the right phase is implemented, emphasizes the stability of the solution.

For more information pertaining to the 'slowness' of ramp and its effect on period doubling; Since the ramp function has too many parameters to characterize, the outlook is to have an experiment with step functions very close to the threshold (for a single drop).

From the above observations the droplet coupling is strong enough to have a discernable effect on the effective acceleration experienced by drop i, given by $\gamma_i(t)$.

$$\gamma_i(t) = \gamma_{exc}(t) + \sum_j \left\{ \gamma_{i,j}(\omega_{exc}) e^{i w_{exc}\left(t - \frac{r_{i,j}}{v_{exc}} + \varphi_j\right)} + \gamma_{i,j}\left(\frac{\omega_{exc}}{2}\right) e^{\frac{i w_{exc}}{2}\left(t - \frac{r_{i,j}}{v_{exc}} + \varphi_j\right)} \right\}$$

$$\gamma_{exc}(t) = -A\omega^2 \sin(\omega_{exc}t)$$

The first term is from the excitation by the shaker (which is at 80 Hz). The effect of other droplets on the ith droplet involves two components. The harmonic component (i.e. at 80 Hz) and the sub-harmonic component at 40 Hz. The harmonic component either lowers or highers the period doubling threshold depending on φ_j (which has been measured, section 3.1). The sub-harmonic component is responsible for the phase selection and symmetry breaking leading to the two stable modes. The sub-harmoinic component is at the same frequency that of the period doubled state. Thus, the phase selection is dependent on the distance between the drops as in the case of a 2λ separation, the droplets go out of phase since the wavefields from both the droplets reinforce each other by constructively interfering each other's wavefield when they are out of phase and negate each other's wavefield by destructively interfering when they are in phase. Below the threshold of period doubling of a single drop, these effects are pivotal in lowering the threshold required for period doubling, due to which reason, configurations with many droplets period double faster. And drops at the center of configurations and surrounded by droplets, period double faster as well. The net vertical acceleration is changed by the presence of a wavefield from the second drop. This is due to the interaction between the droplets which reduces the acceleration that has to be provided by the shaker to attain period doubling. The remaining acceleration is provided by the other droplet. And this trend continues with the case of many droplets, which have a lower threshold when they are together. To summarise, the waves generated by the drops at the excitation frequency of the bath, can add either constructively or destructively depending on their phase (at the stable droplet position) relative to the bath oscillation. These waves are responsible for alleviating the degeneracy in the two period doubled modes by breaking the symmetry of the net excitation. Hence, the period doubling threshold can either be reduced or increased. The wavefield also has waves at subharmonic frequency (half the frequency of the bath/excitation). The phase of these waves decides if they favor either phase A or B.

3.3 Lattice of many droplets

The lattice of many droplets arranged in different configurations at a distance of 2λ on a triangular lattice. In each of these scenarios the droplets interact with one another to arrive at a stable state. The image to the left gives the non-period doubled state and the image to the right gives the period doubled state of the system.
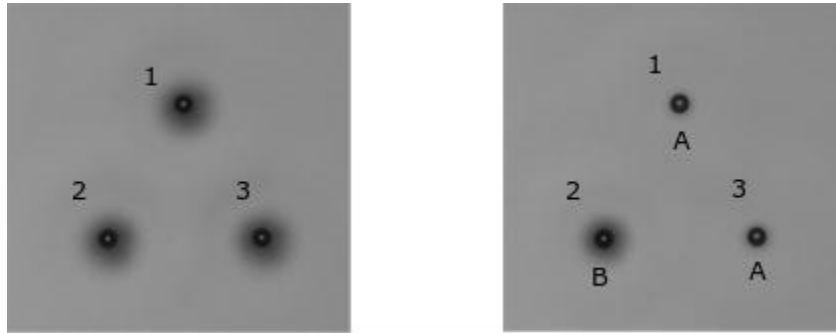
Figure 32: A configuration of three droplets. On the left, before period doubling and on the right, after period doubling.

In Figure 32 we have three droplets, each separated by 2λ. This system does not have a true solution. Every drop wants to be ideally misaligned with every other drop. However, this is not a possibility owing to the geometry. Thus, one of the drops (drop 2, in Figure 32) goes out of phase (phase B) while the other two drops (drops 1 and 3) are in the same phase (phase A). This system has one mistake between drops 1 and 3. However, this is the lowest possible energy for the problem of three droplets. This experiment was repeated multiple times and all the three drops are equally likely to be the one that is out of phase. This helped ascertain absence of any asymmetries with respect to the excitation of the system and size of the droplets. Thus, this further supports the fact that the uncertainty in droplet size is in a smaller range than the order of magnitude that becomes relevant for the process of period doubling.

The phase transition for three droplets was carried out by tracking the gray area around the droplets. The amplitude of the shaker was suddenly increased beyond the threshold for period doubling. The evolution of phase was very discernable, given in Figure 33. Drop 1 is the first to period double followed by Drop2 and then finally Drop 3. When Drop 1 chooses to go out of phase (+1), Drop 2 goes out of phase (-1) with Drop 1. Drop 3 is the last to choose and it can either take phase +1 or phase -1 (both of which have been observed), here it picks phase +1. The solution has three

degenerate states wherein one of the drops, either Drop 1, Drop2 or Drop 3 pick the different phase compared to the other two.
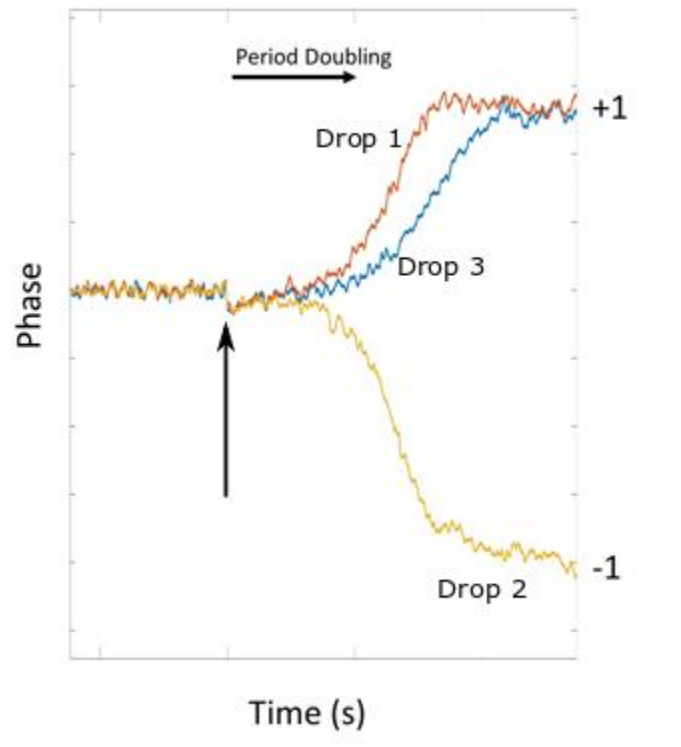

Figure 33: Evolution of phase as a function of time. The yellow line represents Drop 2, the blue line represents Drop 3 and the orange line represent Drop 1. The arrow marks the point in time, at which the amplitude was suddenly increased to beyond the threshold for period doubling.

This indicates that the droplets are communicating with one another to arrive at the solution. This is seen more apparently in the case of larger configurations as well.
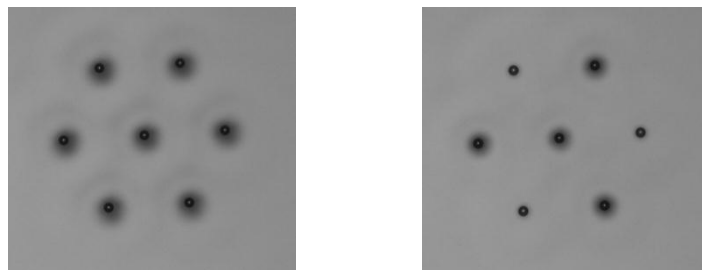
Configurations of different number of droplets:

Figure 34: A lattice of seven droplets forming a hexagon. (Left) Before period Doubling and (Right) after period doubling.

46

Seven droplets in Figure 34 (Left) interacting with one another to arrive at the solution Figure 34 (Right). The configuration of seven droplets has four degenerate states, this is depicted in Figure 39 of section 3.4. The phases are again distinguishable by the gray ring around the drops. The number of mistakes here are 3 of the first order i.e. first nearest neighbours, every droplet wants to be out of phase with every other droplet ideally.
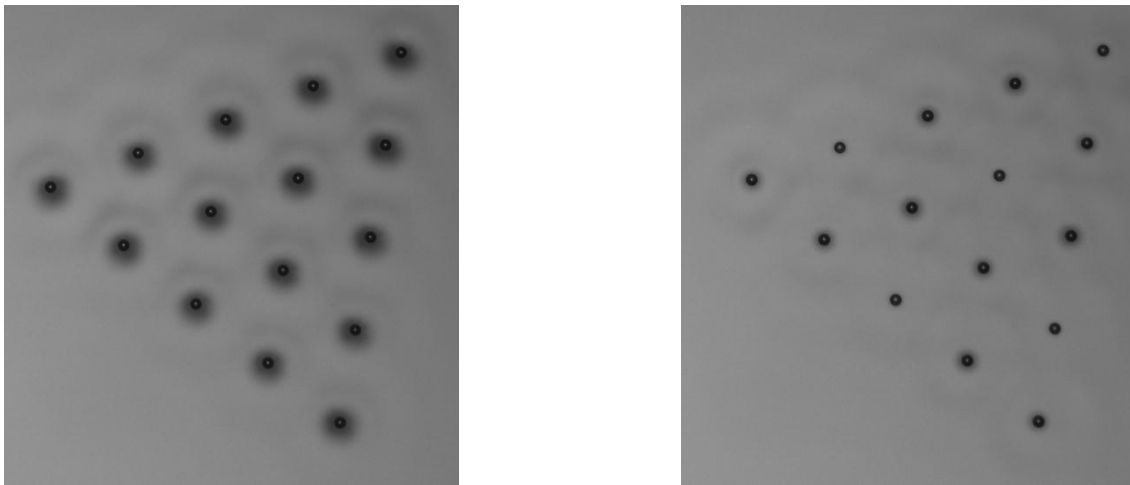
Figure 35: Lattice of 15 droplets forming a triangle. (Left), BPD and (Right) APD.

Lattices in the same shape can have different results, as demonstrated by lattices of 15 drops and 10 drops in Figure 35 and Figure 36. The number of mistakes here are 10. Even though there are ten apparent mistakes of the first order, in this geometry the least energetic state is given by the phase configuration obtained.

Figure 36: Triangular Lattice of 7 droplets forming a triangle. (Left), BPD and (Right) APD.

Hexagonal structure of 19 droplets given in Figure 37. The lowest energy state has 12 mistakes of the first order.
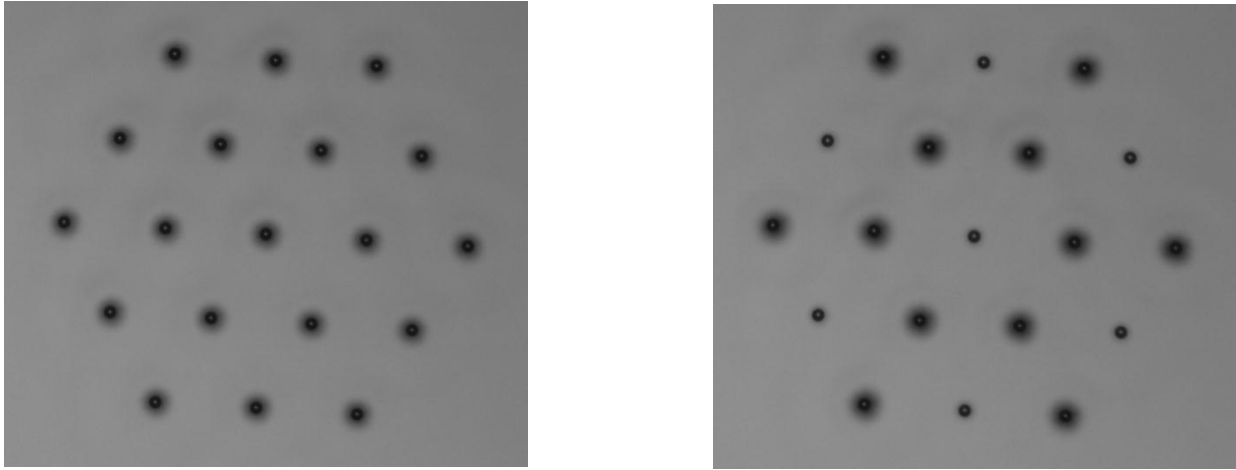
Figure 37: Hexagonal geometry with a lattice of 19 droplets. (Left) BPD and (Right) APD
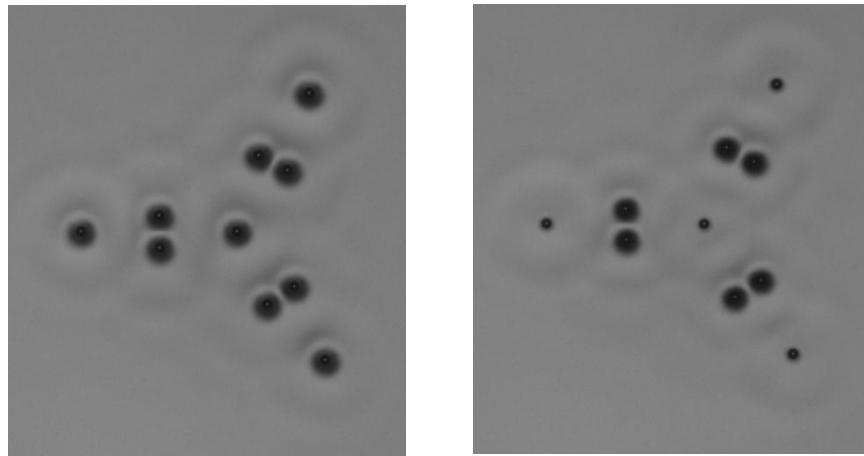
Figure 38: 10 droplets arranged at various stable distances.

Figure 38 represents a configuration with all three possible stable distances. The final configuration has zero first order mistakes. All the droplets have the expected phase configuration.

All the configurations after period doubling correspond to the minimum energy state, which were verified by the simulations, given in section 3.4. This makes for a compelling system for more detailed study owing to the two possible outcomes of the drops, the reproducibility of the process, interaction between the drops leading to intriguing outcomes, and interesting dynamics between the drops and the surface.

3.4   Ising model for bouncing drop lattices

The Ising Hamiltonian is given by:

$$H = -\sum_{i.j} I_{i,j}\sigma_i\sigma_j$$

The interaction term magnitude was given by the envelope of the wavefield which varied as a function of the distance between the droplets. The sign of the term was given by the distance between two droplets as explained in Table 2.

Table 2: Tentative mapping for designing an Ising Hamiltonian

Ising Machine ⟵	⟶ Our Droplet Machine
1. Minimises energy of a lattice of spins σ_i which can be in {+1/-1} state.	1. Minimises "energy" of a lattice of phases; A = +1 and B = -1, after transition to period doubling.
2. Energy: H = $-\sum_{i,j} I_{i,j}\sigma_i\sigma_j$	2. Energy: H = $-\sum_{i,j} I_{i,j}\sigma_i\sigma_j$
3. Interaction $I_{i,j}$ mediated electromagnetically.	3. Interaction $I_{i,j}$ mediated through surface waves.
4. $I_{i,j}$ positive: Spins want to align (ferromagnetic interaction). $I_{i,j}$ negative: Spins want to anti-align (antiferromagnetic interaction).	4. $d = (2n+1)\lambda$: phases want to align. $d = 2n\lambda$: phases want to anti-align

The envelope of the wavefield function was given by the form: $f(r) = \left(\frac{a}{\sqrt{r}}\right)(e^{-br})$ The droplets act as sources and produce waves radially, they can be described by the Bessel function [1]. The wavefield envelope was fit to $\left(\frac{a}{\sqrt{r}}\right)(e^{-br})$ as given in section 3.1. The fit parameters obtained were used to simulate the interaction between two droplets. The fit before period doubling was used since the droplets experience the before period doubled state's wavefield close to the transition. Both the fits are very close in value (just before and just after period doubling). If the distance between two drops was λ or 3λ, the interaction is ferromagnetic (as described in section 3.2) and

the interaction sign is taken to be positive and for a distance of 2λ, the interaction term is taken to be negative. The results obtained were consistent with the all the experiments with different configurations. One example of which is demonstrated in Figure 39, the energy of the configuration is plotted along the x-axis with the configurations on the y-axis.

The configurations of droplets were constructed on a triangular lattice with the coupling given by the interaction term for the analysis. In order to check how strong this coupling was, the simulation was carried out for just the first nearest neighbours. The results obtained matched the experimental results for a lattice constant of 2λ.
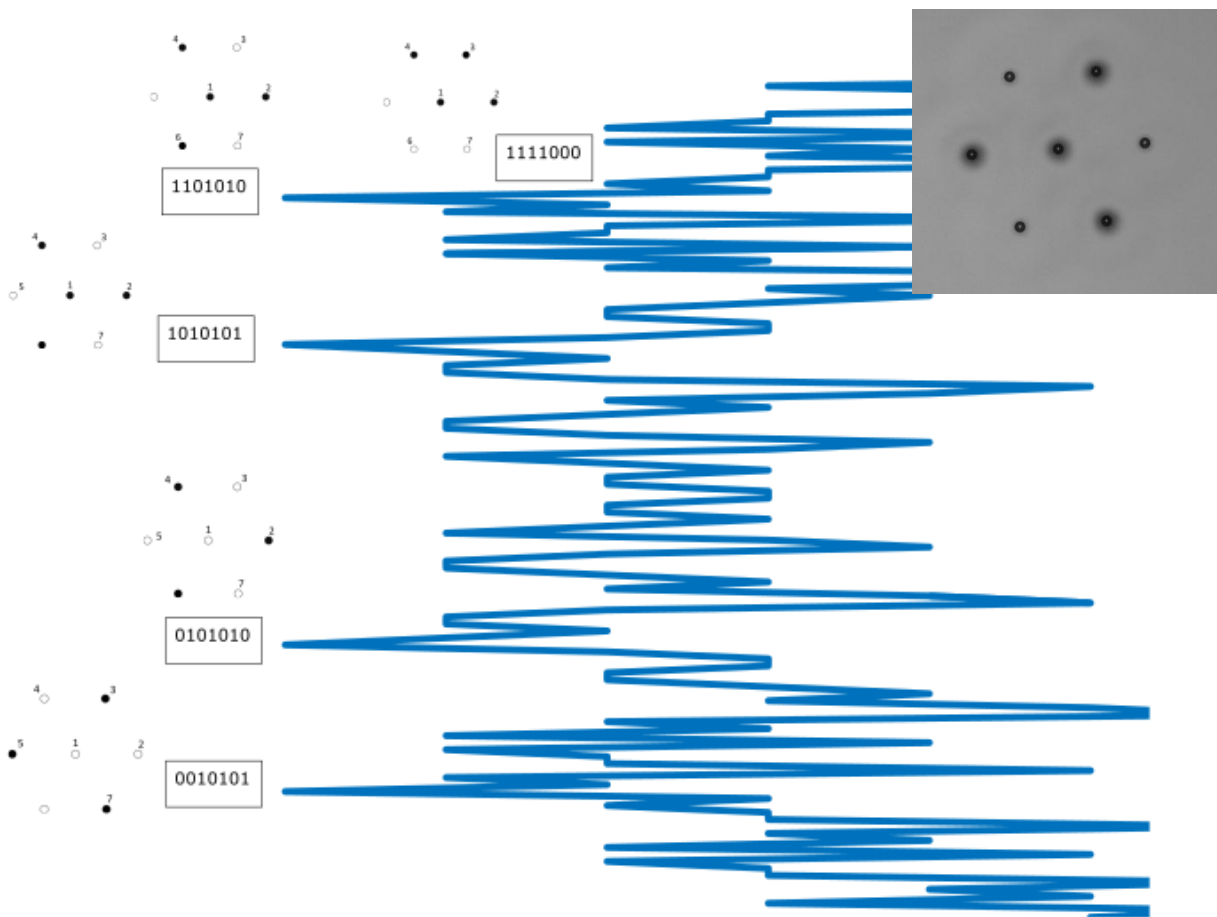

Figure 39: Hamiltonian space with the x-axis representing energy and y-axis being the configuration. The phases of the drops are depicted by 1(s) and 0(s) whose order corresponds to the arrangement of drops depicted in the figure insets. The actual experimental result is given in the top, right.

3.5　Moving droplets to intermediate distances: preliminary experiments
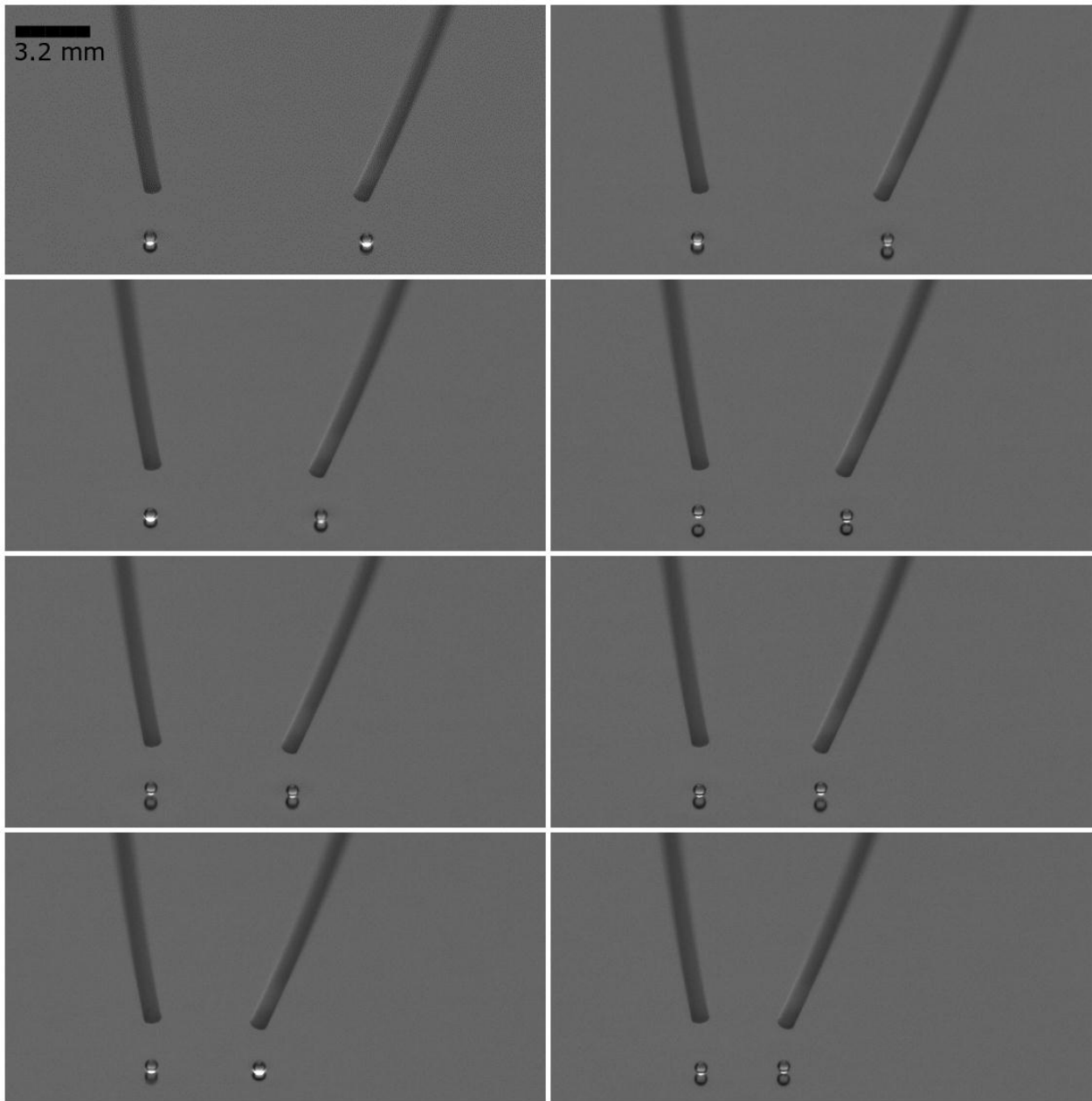
Figure 40: Montage of droplet 2, on the right, at different distances from droplet 1, on the left. Droplet 2 is moved using an electrostatically charged Teflon tip.

The droplets were moved to different intermediate distances as shown in Figure 40, using an electrostatically charged Teflon tip. This induced a dipole moment on the drop, attracting it. This method would be efficient only if the amount of attraction is the same for both the drops which is not possible without having a constant voltage source.
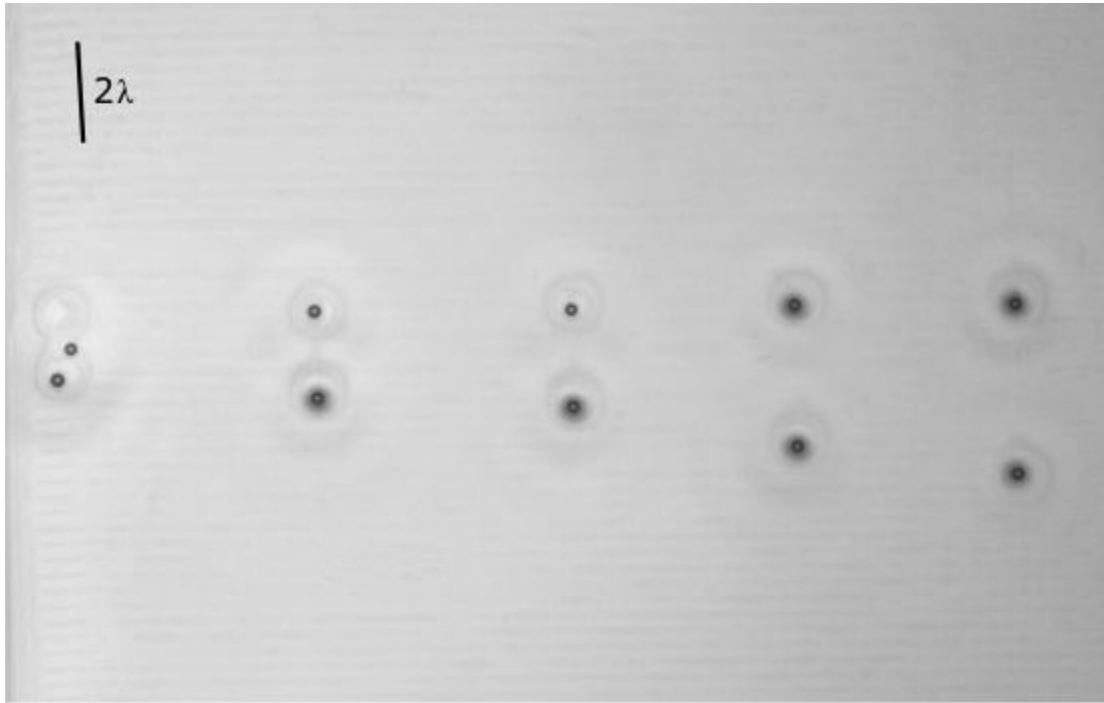
Figure 41: Drops placed at unstable distances in wells. The distance was varied from >3λ to <1λ.

In Figure 41, the droplets are trapped in wells. This was achieved by suitably tuning the bath height. This reduced the coupling between droplets, allowing them to reside at intermediate distances. The wells were 3D printed at distances between 3λ and 1λ. The very first pair have a stronger interaction, due to their proximity, that overcomes the barrier and move them to the first stable state of λ. This is not an ideal system since the wells limit the interaction between droplets to a great extent. The outlook of this project will involve finding a suitable method to tune distances between droplets.

To summarise, the droplets were fixed at a position by placing wells in the bath and having a shallow layer of oil above these wells. As long as the wells are homogeneous, the interaction uniformly changes for all drops. The droplets remained at different unstable locations in the presence of these wells. This is a trade-off in terms of the strength of coupling between the droplets. The method involving electric field is to be explored.

4   Conclusion and Outlook

On the whole, this problem was very rich in terms of exposure to different techniques. The method of wavefield imaging can be implemented on any transparent surface whose curvature is to be analysed. Different aspects in image analysis like analysis with sub-pixel accuracy are very versatile in their applications and whose central ideas are relevant in many situations involving detection and tracking.

The set of interacting bouncing droplets behave as a system of synchronized oscillators that are coupled together by the wavefield that they emit on the surface. When bouncing at the excitation frequency, droplets spontaneously self-organize into various stable 2D patterns on the surface of the bath. These positions correspond to a null net horizontal force acting on them during the quasi-contact phase between the drop and the surface of the bath. This occurs when the droplets land at a position in space and in time that does not have a sloping surface due to other droplets. Upon being sufficiently excited, the droplets undergo period doubling and acquire one of two phases with respect to each other. The dynamics involving this transformation was explored. The dynamical coupling between the droplet and the surface is responsible for the process of period doubling. When we have more than one droplet, the phase selection is based on the interaction term which in turn depends on the distance between the drops. The wavefield was measured for a single drop. This was used to obtain the envelope of the wavefield to verify the outcome of many configurations and to reinforce the empirical observations with regard to the phase selection process. The wavefield was simultaneously measured with the vertical motion of the drops for the outlook on the role of subharmonic frequencies in the process of period doubling. The case of a single droplet gave deeper insight into the process of period doubling and the bifurcation of the bouncing period into two modes along with quantified results. The experiments with two droplets looked at the interaction between the droplets. Two droplets at a stable distance, have a period doubling threshold (in terms of the amplitude of the shaker) that is lower than the threshold for a single droplet. In patterns involving many droplets, the droplets at the center, which have stronger coupling due to being surrounded by more droplets, period double for a lower threshold amplitude than in the case of the drops on the edge which experienced interaction with fewer drops. The simulations indicate that the system has strong coupling up to the first nearest neighbor after which the interaction decays due to the damping of the wavefield. But every drop has an effect on every other drop owing

to its influence on the phase selection by the drop closest to it, which later decides the phase of another drop. These interactions give rise to the symmetric phase configurations that are observed. The droplets also compute the solution corresponding to minimum energy by rectifying their phase if the phase does not correspond to the ground state configuration. The droplets were made to period double in phase with respect to each other by increasing the amplitude of the shaker by means of a ramp function and tuning the slope to achieve an example wherein the droplets at 2λ became period doubled with the same phase but rectified their mistake by coming back to the non-period doubled state and finally going out of phase, which is the expected outcome at 2λ. This illustrates the robustness of the system in terms of finding the ground state.

In our system, the distance between the drops which gives a handle on the interaction term is not easily manipulable currently. The drops are at fixed distances corresponding to the points in space that have no slope on the surface when the drop comes in contact with the surface. This limits the range of energy landscapes that can be explored since the number of initial configurations that we can have are limited to the triangular lattice. To vary the distance between droplets, some preliminary experiments were carried out as shown in Figure 40 and Figure 41.

Our system is two dimensional, limiting the mapping to other systems involving spin glasses and most importantly the coupling between drops in our system decays with distance. Beyond $\sim 2\lambda$, the effect of the drops on each other is not prominent.

The work carried out involved the development of new techniques and insight into the key aspects of the system. Both, the ability of these drops to interact and arrive at the ground state and the comprehensive experimental characterisation of this system provide the ideal basis for making an equivalence with the established Ising machines.

5 Appendix

5.1 Growth rate and decay rate of period doubling for one and two drops

Figure 42: Figure on top represents the period doubling for a single drop and figure below represents one drop of a configuration of two drops experiencing a series of step functions in amplitude. The period doubling amplitude (difference in bounce times) higher and decay is rate lower in the two drop case than one drop. Thus, the drops enhance each other's period doubled state.
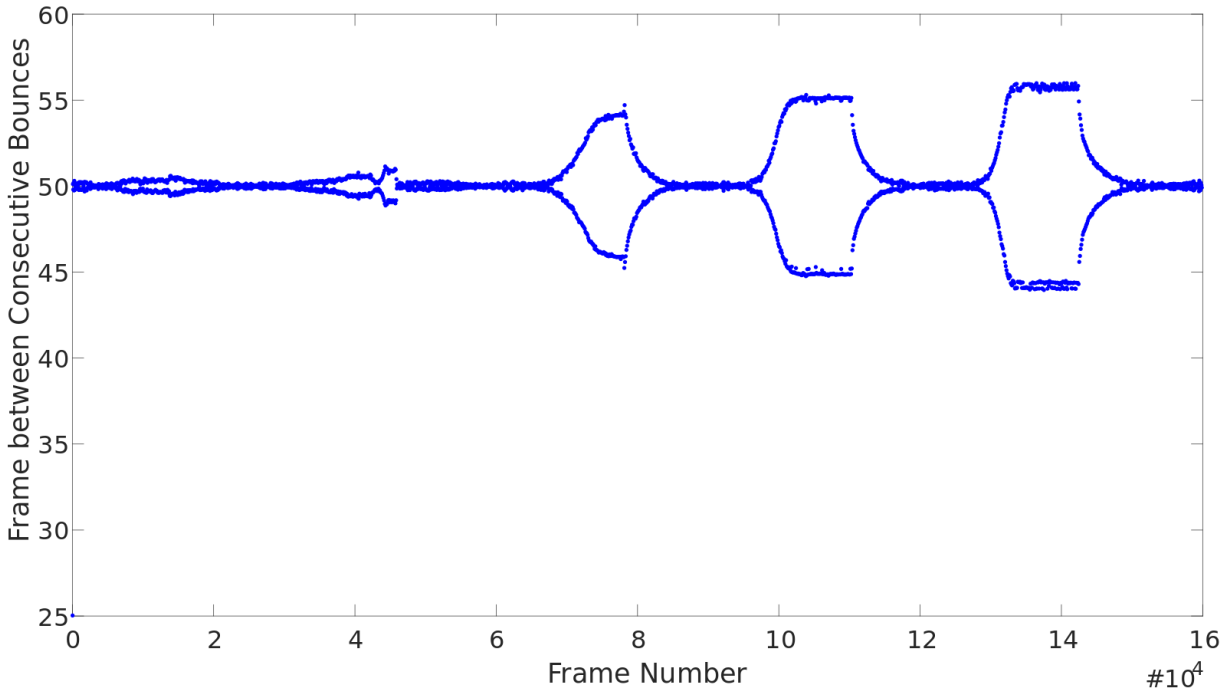
Figure 43: Figure on top represents the period doubling for a single drop and figure below represents one drop of a configuration of two drops experiencing a series of step functions in amplitude (different from previous case). The period doubling threshold is much lower for the two drops case since the drop in the two drop configuration has already period doubled for the same excitation.

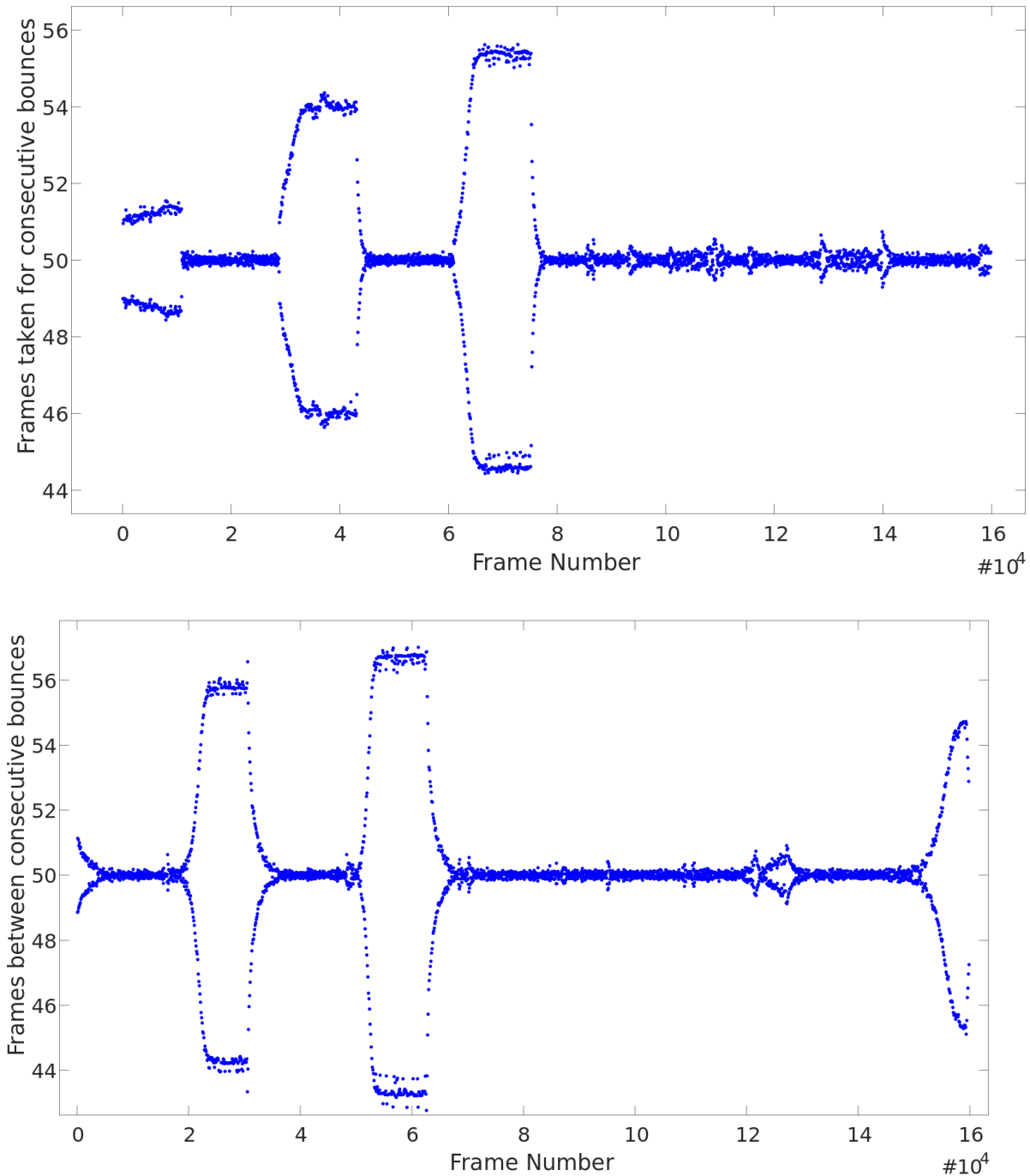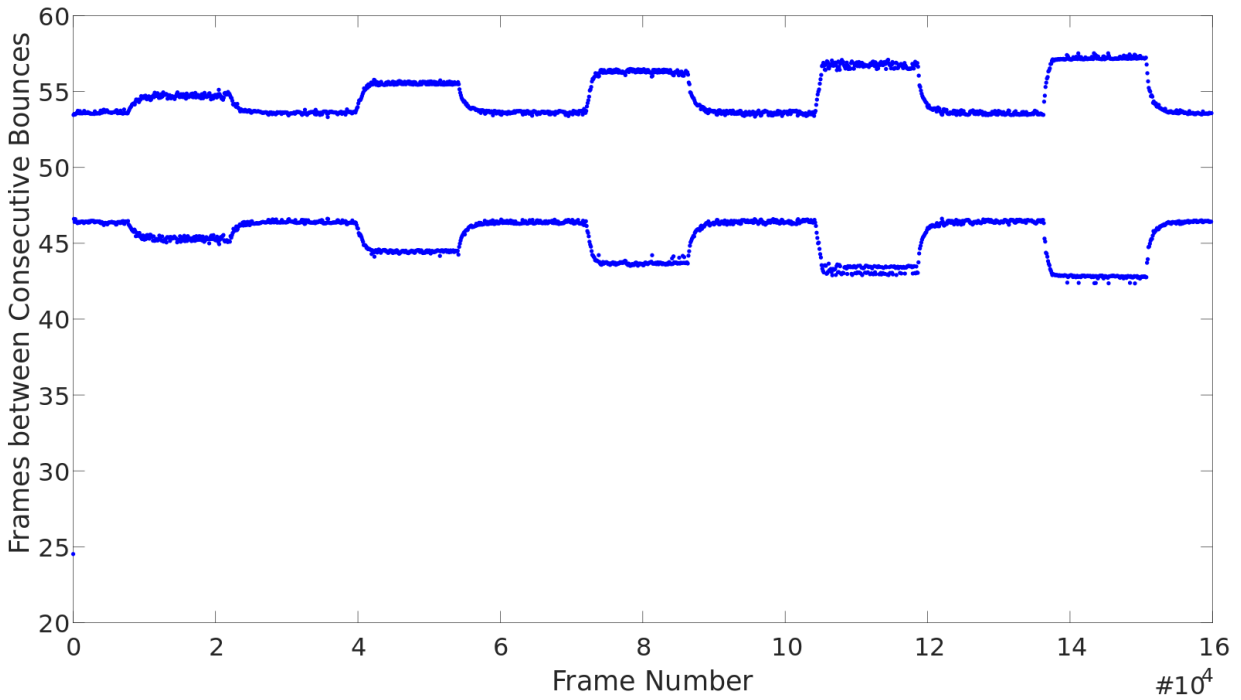## 5.2   Period doubling threshold for one and two drops
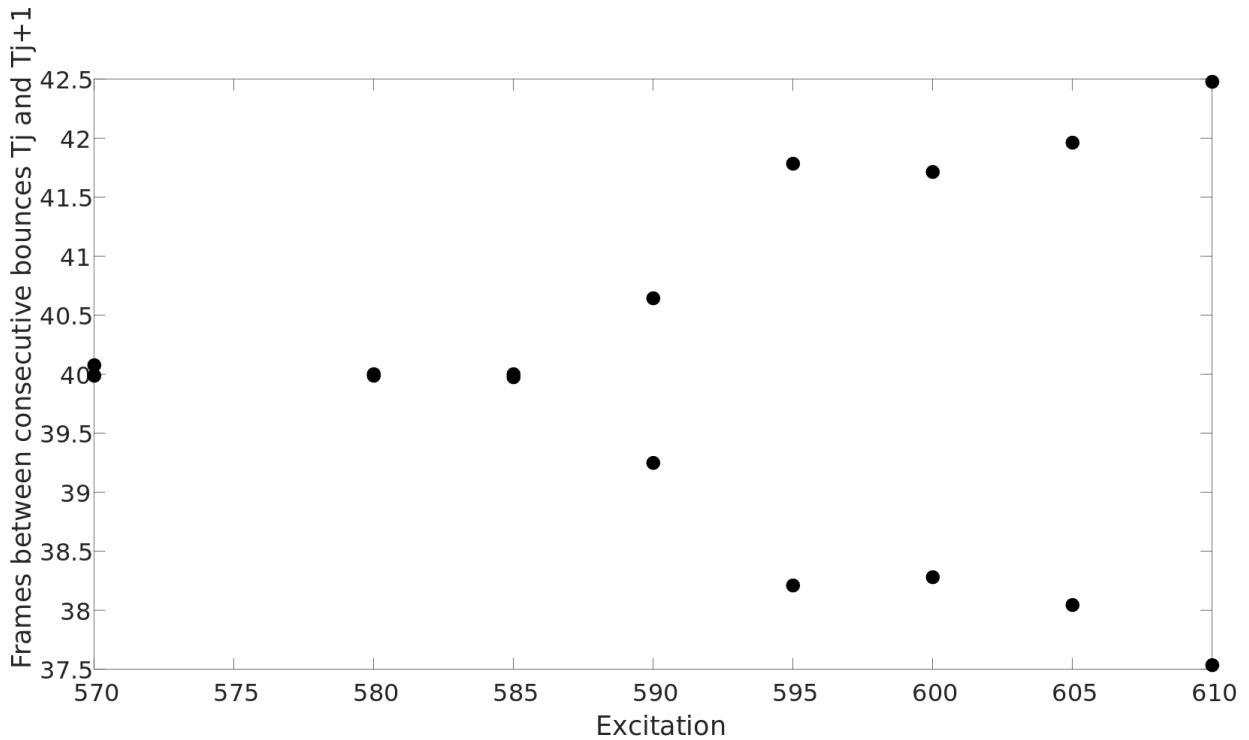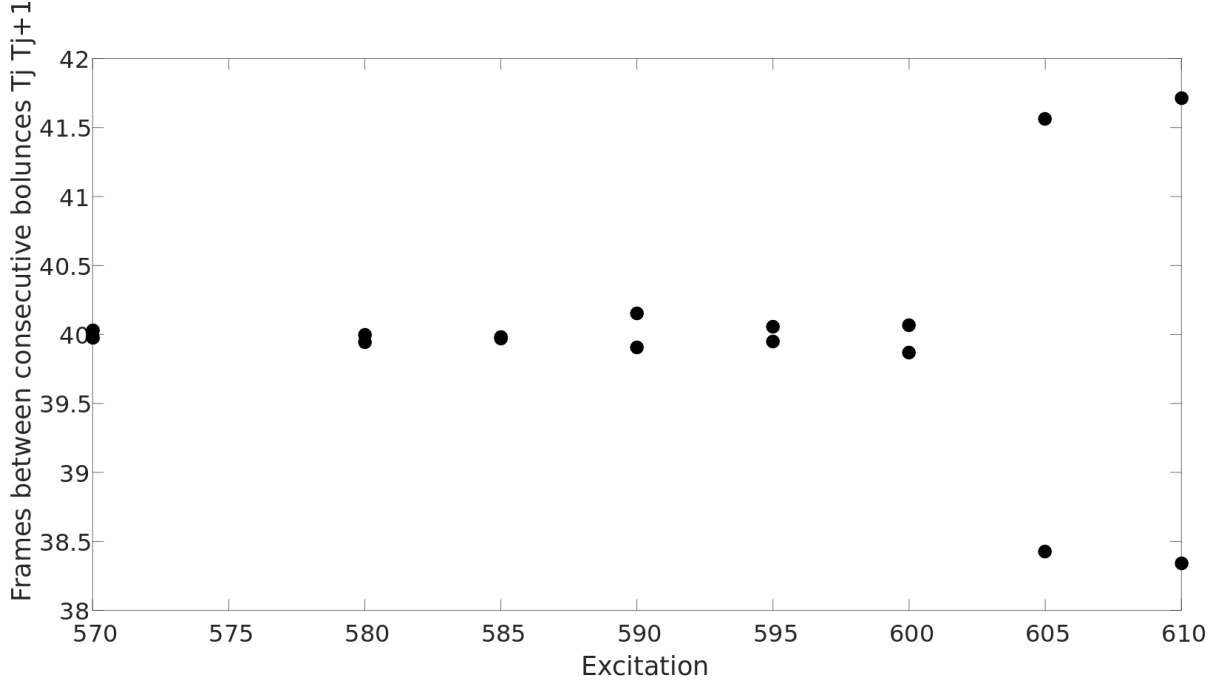
Figure 44: Figure on top represents the period doubling for a single drop and figure below represents one drop of a configuration of two drops experiencing a series of step functions in amplitude, same as for the plots in Figure 44. The period doubling threshold is much lower for the two drops case since the drop (second figure) in the two drop configuration has already period doubled for a lower excitation. X-axis is the voltage (mV) of excitation given to the shaker.

5.3   Mapping to the Max-Cut Problem

Max-Cut: Partitioning a graph G (V,E) with V vertices and E edges, into two sets S and V/S such that the weight of the edges connecting the two sets is maximised.

$G = (V, E)$

$\omega : E \to \Re$ is the weight of the edges

$Cut\ (S, V / S)$ such that

$\max(\sum \eta)$ where η is the set of edges with one

end point in S and the other end point in V/S

Considering $\omega_{jl} = \omega_{lj}$ where $(j, l) \in E$ and

$\omega_{jl} = 0$ if where $(j, l) \notin E$

The weight of the cut S is given by

$$\omega(S) = \sum_{j \in S, l \in V / S} \omega_{jl} = 1/4 \sum_{j, l \in V} \omega_{jl} - 1/4 \sum_{j, l \in V} \omega_{jl} \sigma_j \sigma_l$$

$\sigma_j = +1$ if j^{th} vertex $\in S$

$\sigma_j = -1$ if j^{th} vertex $\notin S$

The Hamiltonian is defined by

$$H = -\sum_{1 \le j \le l \le N} I_{jl} \sigma_j \sigma_l$$

Now if we define $I_{jl} = -\omega_{jl}$,

maximising $\omega(S)$ is equivalent to minimising H

Figure 46: A 5-node graph with 5 equally weighted edges

Figure 45: The solution is 5-Cut

$\sigma_2, \sigma_3 = +1$

$\sigma_1, \sigma_4, \sigma_5 = -1$

The max Cut problem is NP hard. Upon adding nodes/vertices, the computational time scales as a power law.

Designing a penalising function to suit our combinatorial optimisation problem is what constitutes writing the Hamiltonian function. In the Max Cut problem, the penalizing function is basically taxing the conditions wherein the nodes connected by a heavy edge are in the same set. This is the reason we have the factor of (1/4). We have considered $\omega_{jl} = \omega_{lj}$, which gives a factor of (1/2). The other half adds up to one ω_{jl} if $\sigma_j . \sigma_l = -1$, that is, the nodes are in different sets.

For example, if we have 5 nodes connected by equally weighted edges in such a manner as given in Figure 46, the Max Cut solution would be five-cut as depicted in Figure 45.
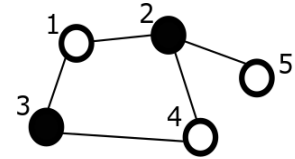
Real World problems which use the Max Cut solution involve image segmentation (separating an object from its background), clustering problems, network analysis, market target audience and basically problems involving picking out data points that are close to each other. S and V/S represent the two sets whose sigma values have the opposite sign.

Figure 47: Three node graph with equally weighted edges followed by all its degenerate solutions and (Right) seven node graph with different weighted edges followed by its solution considering the heavier weighted edges to play a predominant role.

The three-node case with all degeneracies is shown in Figure 47. Thus, in the three-node case, one node should have an opposite sign w.r.t the others. The seven-node case, considering the maximum weighted sides, the nodes 2,4,6, should have an opposite sign to that of 1,3,5,7. The node 7 can be either in S or V/S. There are four degenerate pairings of the vertices, as expected from Figure 39.

5.3.1   Mapping the Hamiltonian to our system

$$H = -\sum_{i,j} I_{i,j}\sigma_i\sigma_j$$

Now, say our coupling is negative. i.e. $I_{i,j} < 0$.

The coupling is anti - ferromagne tic.

And the product $\sigma_i\sigma_j < 0$ to have a negative H.

Let the weight of the nodes be defined by

$\omega_{ij} = e^{-ar}/\sqrt{r}$ where r is the distance between th e nodes.

For the ith node, if $\sigma_i = +1$ then the ith node $\in S$

otherwise, the ith node $\in V/S$.

59

These are the cases at 2λ, for the first λ and third 3λ stable distance, the droplets are all in phase after period doubling. This is evident from looking at the interaction term which is positive i.e. ferromagnetic interaction. And from above, we know $I_{jl} = -\omega_{jl}$. Thus, the total weight $\omega_{jl} < 0$.

Thus, maximising the weights across two sets is nothing but having the total weight equal to zero (any edge connecting two sets will give a negative value). Thus, all the drops are in the same phase i.e. all nodes belong to one set.

6 Bibliography

[1] Eddi, A. (2011). Marcheurs, Dualité onde-particule et Mémoire de chemin (Doctoral dissertation, Université Paris-Diderot-Paris VII).

[2]   Couder, Y., Protiere, S., Fort, E., & Boudaoud, A. (2005). Dynamical phenomena: Walking and orbiting droplets. Nature, 437(7056), 208.

[3] Protière, S., Boudaoud, A., & Couder, Y. (2006). Particle–wave association on a fluid interface. Journal of Fluid Mechanics, 554, 85-108.

[4] Couder, Y., & Fort, E. (2006). Single-particle diffraction and interference at a macroscopic scale. Physical review letters, 97(15), 154101.

[5] Protière, S. (2007). Gouttes rebondissantes: une association onde-particule à échelle macroscopique (Doctoral dissertation, Université Paris-Diderot-Paris VII).

[7] Pierański, P. (1983). Jumping particle model. Period doubling cascade in an experimental system. Journal de Physique, 44(5), 573-578.

[8]   Eddi, A., Decelle, A., Fort, E., & Couder, Y. (2009). Archimedean lattices in the bound states of wave interacting particles. EPL (Europhysics Letters), 87(5), 56002.

[9]   Fabre, C. (2014). Optical computing: The optical Ising machine. Nature Photonics, 8(12), 883.

[10]   Lucas, A. (2014). Ising formulations of many NP problems. Frontiers in Physics, 2, 5.

[11] Utsunomiya, S., Takata, K., & Yamamoto, Y. (2011). Mapping of Ising models onto injection-locked laser systems. Optics express, 19(19), 18091-18108.

[12] Goto, E. (1959). The parametron, a digital computing element which utilizes parametric oscillation. Proceedings of the IRE, 47(8), 1304-1316.

[13] Marandi, A., Takata, K., Wang, Z., Byer, R. L., & Yamamoto, Y. (2014, June). Network of femtosecond degenerate OPOs for solving NP-Hard Ising problems. In CLEO: QELS_Fundamental Science (pp. FM2A-1). Optical Society of America.

[14] Inagaki, T., Haribara, Y., Igarashi, K., Sonobe, T., Tamate, S., Honjo, T., ... & Tadanaga, O. (2016). A coherent Ising machine for 2000-node optimization problems. Science, 354(6312), 603-606.

[15] Takata, K., Marandi, A., Hamerly, R., Haribara, Y., Maruo, D., Tamate, S., ... & Yamamoto, Y. (2016). A 16-bit coherent Ising machine for one-dimensional ring and cubic graph problems. Scientific reports, 6, 34089.

[16] Wildeman, S. (2018). Real-time quantitative Schlieren imaging by fast Fourier demodulation of a checkered backdrop. Experiments in Fluids, 59(6), 97.